Two-Color Chirped-Pulse Amplification Fiber Amplifier, for Mid-Infrared Generation

by

Alaa Mohammed Al-kadry

A thesis
presented to the University of Waterloo
in fulfillment of the
thesis requirement for the degree of
Master of Science
in
Physics

Waterloo, Ontario, Canada, 2010

AUTHOR'S DECLARATION

I hereby declare that I am the sole author of this thesis. This is a true copy of the thesis, including any required final revisions, as accepted by my examiners.

I understand that my thesis may be made electronically available to the public.

Abstract

The goal of this thesis is developing a two-color Ytterbium (Yb) fiber amplifier system that can be used for generation of mid-infrared radiation. Previously, our group reported generating 20 µW of average power, at a wavelength of 18µm. This was accomplished through the amplification of a two color-seed with peaks at 1040nm and 1110nm, through a two stage amplification without any compression. The mid-infrared radiation (MIR) was generated with a 4.5 ps pulse duration by the method of difference-frequency mixing, using 300 mW of average power from the two-color Yb-fiber amplifier. Because there was no limitation by two-photon absorption, MIR output power could be scaled by increasing the amplifier power. The current project aims to increase the peak power of the laser pulses to improve the efficiency of the nonlinear mixing. The two-colour seed is generated by continuum generation in a photonic crystal fibre, pumped by 200 mW of average power from a mode-locked Yb:fibre laser. In order to efficiently increase the energy of the two wavelengths, the 4.6 mW seed pulse is now pre-amplified up to 21 mW in a 2.7 m length single mode, single core Yb:fibre . The pre-amplifier used a double-ended pumping scheme with two single mode diode lasers at 976 nm each having 150 mW maximum pump power. A notch filter was placed in the output beam to eliminate any Amplified Spontaneous Emission. After further amplification in a 7 m length of double clad, Yb-fibre, a maximum average power of 727 mW was achieved for two colours peaked at 1035 nm and 1105 nm wavelengths. The pump power for this stage was 6 W. A grating stretcher is now used to select the two-colour input along with stretching the pulses. A three grating compressor is used to compress the output pulses to 466 fs pulse duration. After compression the average power of the two colours is 350 and 110 mW for wavelengths at 1035 and 1105nm, respectively. These higher power pulses are planned to be used to increase the mid-infrared generation efficiency.

Acknowledgements

Firstly, my great gratitude goes to Dr. Donna Strickland, my supervisor, for her unlimited support. I am deeply indebted to her, she taught me how to be patient in research, and how to seek results. Under her guidance I had the opportunity to participate in conferences that have advanced my professional skills and experience. Her confidence in me and her endless encouragement has motivated me to work hard during the study.

I would like to express my sincere thoughts to all of those who helped me to carry out this graduation project. I wish to thank Phillip McNelles for his contribution in the development of this experiment.

I would like to thank Dr. Joseph Sanderson, Dr. Li Wei, and Dr. Donna Strickland for being on my defense committee. I also wish to thank Dr. Kostadinka Bizheva for being on my Masters committee these last two years.

I would like to thank my father and mother for their support and encouragements. Also, I sincerely thank my uncle for his help and the support he gave during the last two years. Thanks should be also addressed to my brother and sisters.

Table of Contents

List of Figures

List of Tables

Chapter 1

Introduction

A dual-wavelength, fiber laser based on supercontinuum (SC) generation, Chirped Pulse Amplification (CPA) and Ytterbium (Yb^{3+}) doped fiber amplifiers acting at a two colors of seventy nanometers apart (1035 & 1105 nm) is built to generate a mid-infrared radiation of 18 μm wavelength by a nonlinear process called difference frequency mixing (DFM). The nonlinear process is proportional to the intensity of the two colors. For this reason, increasing the energies and shortening the time duration of the two colors will allow a more efficient nonlinear process, i.e. a higher power of the generated mid-infrared radiation.

Beginning with a ytterbium fiber laser oscillator at 1030 nm, a photonic crystal fiber (PCF) was used to broaden the laser seed spectrum into hundreds of nanometers, a free-space three-grating stretcher to stretch and select the two colors, a single-mode, single-clad preamplifier to increase the seed energy, a double-clad fiber amplifier doped with ytterbium, along with a high power pump diode at 975 nm, and finally a three grating compressor to recompress pulses, the dual-wavelength fiber laser system was constructed. With enough amplification through multi-stage configuration, a two color radiation with 1.8 W average power was obtained which should allow the generation of hundered of microwatts of mid-infrared radiation at 18 μm.

1.1 Two-Colour Lasers

Laser sources nowadays are able to generate ultrashort pulses of intense radiation from the visible up to the near IR-regions. The range of the emitted laser wavelength is limited by the finite gain bandwidth of the gain medium and the cavity mirror bandwidth in the laser

cavity. The gain medium of these lasers can be gas, crystal, liquid, glass, or doped fiber.

For doped-fiber lasers, silica fibers can be doped with a variaty of rare-earth materials (Ytterbium, Erbium, etc.). Ytterbium (Yb^{3+}) fiber, for instance, can produce lasing radiation at 0.9 to 1.15 μm wavelength range. While for crystal lasers, Ti:sapphire crystals can exhibit a broad gain profile from 650 to 1100 nanometers. However, to further increase the wavelength range of laser sources, a non-linear frequency mixing optical process is necessary.

The broad gain bandwidth profile makes it possible to generate a tunable dual-wavelength laser as well; a laser that operates simultaneously at two frequencies.

Dual-wavelength lasers are promising laser sources for many applications, such as Difference frequency generation (DFG). DFG requires two laser sources, where a mid-infrared radiation can be produced by using a nonlinear crystal. A high degree of accuracy of geometrical and temporal adjustment are required in the nonlinear crystal. It is for this reason that dual-wavelength operation in a single laser is attractive for such a process. A number of approaches are being explored to reach this goal.

The Ti:sapphire laser is the most widely tunable laser resource ever known. And with its broad tuning range and large stimulated emission cross section, it is ideal for producing more than one wavelength simultaneously. Historically, two approaches were followed to achieve a dual frequency operation of Ti:sapphire. The first approach to realize dual-wavelength was obtained by selecting and amplifying the two colors within the laser cavity. This method included double-prism-dispersion cavity, two-mirror-resonator with birefringent filter (BRF) as its tuning instrument, or two independent seeds injection. This approach was about building a dual-wavelength oscillator.

Following this approach, the first dual-wavelength Ti:sapphire laser operating in continuous wave (cw) state and pumped by an Ar^{+}laser at 714 and 845 nm wavelengths (121nm seperation) was reported by Richard Scheps and Joseph F. Myers [1]. A modest 80 mW average output power was produced from this laser. One year later, a more powerfull and mode-locked dual-wavelength laser system were developed by many groups [2, 3, 4]. Leitenstorfer et. al. in 1995 developed a two-color Ti:sapphire laser where the two pulses are independently tunable over a wavelength interval as wide as 100 nm and with pulse durations below 30 fs [5]. By injecting two independent seeds into the laser cavity, a dual-wavelength output spectrum at 763 and 784 nm separation (21nm separation) with 13 mJ average output energy was obtained [8]. Also, lasers characterized by Q-switched operation, delivered a maximum output power of 4.8 W at 744.8 nm and 860.9 nm (116.1nm separation) by pumping the gain medium with a frequency doubled Nd: YAG laser of 23

W and a repetition rate of 6.3 KHz [9]. To generate the two colors of the system, a birefringent filter (BRF) was inserted in a two-mirror-resonator. This gave higher power and ensured the emission of a two collinear wavelengths. Nevertheless, using this filter limits the separation between the two wavelengths, which cannot be changed after fabrication. Furthermore, when the net gain of one of the two wavelengths is lower than that of the other while rotating the filter Continuously to tune the two colors, the two wavelengths turns to be only one wavelength. However, it should be mentioned that the pulse duration of these lasers is relatively long (nano- to micro-second pulse duration).

The other approach was about amplifying the a dual-wavelengths in an appropriate amplifiers. This was achieved by using Ti:sapphire regenerative [10, 11] and multi-pass amplifiers [12]. These systems provided shorter pulses in the femtosecond range, and higher total output energy with more control over the output wavelength separation of the two color spectrum. With a careful gain control of the two-color pulses during amplification, Xia et. al. demostrated a two-color amplifier comprising a regenerative and multi-pass amplifiers to produce 15 mJ total ouput energy which was evenly split between 800 and 870nm wavelengths each of 8 nm bandwidth [12]. The tuning range of wavelengths in this laser was from 800-890 nm limited by the cavity mirror bandwidth. In 2006, Yamakawa developed the highest-energy (5 mJ) two-color chirped-pulse regenerative amplifier (RA) with the largest wavelength separation up to 120 nm [11]. This laser was a Ti:spphire ring regenerative amplifier which produced two pulses at 740 and 861 nm. Both dual-wavelength lasers of ref. [10, 11] were used to generate mid-infrared radiation via DFM process.

However, building the amplifier system of Ti:sapphire lasers requires a careful alignment of the beam to extract the maximum gain from the lasing medium. Besides, a regenerative and multipass amplifiers are necessary to achieve a high gain (several watts output power) which relatively has complex schemes. Because of this, fiber-based lasers are more preferable as they can provide high gain efficiency over a broad bandwidth, and an inherent compactness as the complete integration of the laser process takes place in a waveguide, which by turn leads to the production of high-brightness high-power laser system. The ultrabroad bandwidth covered by fiber lasers can be selected by the appropriate doping materials. For instance, Yb:doped fiber (YDF) laser systems are the most selected for developing a dual-wavelength fiber laser as it provides a high gain efficiency and a broad gain profile.

In the work involving the use of a Ti:sapphire as laser oscillator and Yb-fiber as the laser amplifier, Dongfeng et. al. [13] developed a fiber amplifier which generates dual-

wavelength pulses at 1042 and 1100nm; a 58nm separation wavelength of 450 mW average output power. This power level was achieved by using a 6m double-clad fiber preamplifier and a 10m fiber-length amplifier. Further wavelength separation of 60nm was obtained by Budz et. al. [14]. The compact dual-wavelength source was developed from a single YDF amplifier and synchronized semiconductor seed lasers operating at wavelength differences of up to 60 nm. Also, by using a mode-locked Yb:fiber seed oscillator, Romero-Alvarez et al. [15] demonstrated the generation of a two color fiber amplifier with more wavelength separation (65nm). Two stages of amplification using double-clad fibers was employed to obtain a 300 mW output average power at 1038 and 1103 nm . On the other hand, a continuous-wave (CW) diode lasers was utilized by Goldberg to seed separate Yb-doped and Er-doped fiber amplifiers, generating signals at 1.1 μm and 1.5 μm. The two colors were amplified using different fiber lengths and rare-earth dopants to achieve an optimal gain for the two pulses [16].

In addition to the mentioned types of lasers, another approach of developing a dual-wavelength laser was made by using nonlinear crystals, such as potassium titanyl phosphate (KTP) or $LiTaO_3$ crystals [17]. The two colors are produced via a parametric down conversion process of a strong pump laser in a suitable medium in an optical parametric oscillators (OPOs). This interaction can be described as a stimulated inelastic scattering of a pump photon by the crystal, where a pump photon of frequency ω_p is absorbed and two new photons with frequencies ω_s and ω_i known as signal and idler photons are generated, respectively. However, this nonlinear process necessarily leads to average powers much less than the OPO pump laser (the Ti:Sapphire laser), making it less efficient for generating mid-infrared radiation above 10 μm wavelength.

1.2 Fiber Chirped Pulse Amplification

In these high-peak-power, dual-wavelength laser systems, pulses are amplified until it begins to incur one of several nonlinear problems associated with intense light. At high optical intensities, materials begin to explicitly show the dependence of their index of refraction on intensity (Kerr effect). This by turn determines the phase velocity of light and therefore a beam with a Gaussian intensity cross-section (non-uniform intensity distribution) suffers a delay of phase at the beam edges where the rate of change of intensity with time is significant. This is known as self-focusing. This change of phase of light waves degrades the ultimate capacity of light to brought to a focus.

In typical high-power short-pulse laser systems, it is the peak intensity, not the energy or the fluence, which causes pulse distortion or laser damage. In order to avoid this phase distortion, chirped pulse amplification (CPA) is used to lower the peak-intensity of pulses before amplification [18]. A grating stretcher dissects a laser pulse according to its frequency components, and reorders it into a time-stretched lower-peak-intensity pulse of the same energy[19]. The stretched pulse can then be amplified safely to high energy to be finally recompressed through a complementary arrangement of parallel diffraction gratings (compressor) [20], and thus resulting in a very short pulse of enormous peak power; a pulse which could never itself have passed safely through the laser system.

For Fiber Chirped pulse amplification system, rare-earth doped silica fibers are being used as the gain medium of the amplifier. The core is doped, usually with rare-earth atoms (ytterbium, erbium, thulium, etc.) which have distinctive absorption and emission spectra. To act as a gain medium, the pump laser source is generally applied at a wavelength for which the fiber dopants have a high absorption cross section. This excites fiber dopants to upper states of relatively long spontaneous radiative lifetimes (meta-stable state). To amplify a laser signal, or a seed beam, the fiber should have a high emission cross section at the signal wavelength. In other word, the seed should create enough stimulated emission as it propagates down the fiber resulting in a seed gain. The drawback of this process (as well as in Ti:sapphire) is the production of ASE independent to the seed. It is an unwanted effect in fiber amplifier as it limits the gain. Such problems can often be controlled by taking a special attention to fiber length and doping level.

As a need arose for more powerful fiber amplifiers, double-clad fibers were manufactured. Adding to single-clad fibers a new layer, known as the inner-cladding, allowed efficient launch of pumping despite their poor beam quality. The inner cladding has a much larger area than the core layer. This considerably produced more gain than was previously possible in single-clad single mode doped fibers.

However, after this invention it did not take long before strong fiber nonlinearity caused nonlinear distortion to the output amplified spectrum. To overcome this, two approaches were followed in ultra-short fiber amplification. The first was based on careful control of linear and nonlinear impairments inside fibers, known as parabolic pulse amplification, while the other is CPA.

In a solid-state amplifier, CPA was employed by stretching pulses up to 1 ns duration. This was sufficient to extract energies up to the tera-watt power level without the limitations of the nonlinear effects [21, 22]. Nevertheless, the situation is quite different

for fiber amplifier with length 100 times longer than solid-state amplifier and with mode area at least 100-1000 times smaller. Due to this fact, even 1ns pulse stretching limit the maximum achievable energy from a fiber amplifier due to SPM and Raman gain nonlinear effects. Because the strength of these nonlinear effects is inversely proportional to the optical wavelength, it is easier to extract higher energies for longer wavelength pulses. However, to acquire this amount of stretching a large free space area is needed to build this system.

One step towards a more compact system is to use a combination of a fiber- or linearly chirped fiber grating stretcher and a conventional grating compressor. The main difficulty encountered with this system is the mismatch of all dispersion orders between a fiber or a fiber grating stretcher and a diffraction grating compressor. This prevented achieving bandwidth-limited pulses duration. However, by using this type of laser system a 10 W average output power was demonstrated in 2000 [23]. The laser consisted an all-fiber ultrashort-pulse seed laser, a short length single-mode fiber stretcher, a 4.3m length of 25 μm diameter core double-cladding Yb-fiber amplifier, and a grating pulse compressor. The importance of this result is that such a power level significantly exceeds average powers achievable with conventional mode-locked Ti:Sapphire lasers. Fiber-based CPA systems are therefore most suitable for high pulse repetition rates combined with high average powers. During the later years, average powers of hundered of watts were generated [24, 25, 26].

To fully benefit from the compactness of fibers, chirped fiber Bragg gratings [27], Chirped quasi-phase matching (QPM) gratings and volume Bragg gratings were also used as femtosecond-pulse stretchers and compressors. It should be mentioned with respect to extract the highest saturation-fluence limited energies from a fiber based system, none of the compact devices can fully replace conventional diffraction grating arrangements.

1.3 Super-Continuum Generation

A short duration laser pulse with sufficient energy can be used to generate a pulse of very broad spectral bandwidth -the supercontinuum- by passing it through a medium whose refractive index varies with the square of the incident electric field.

Supercontinuum (SC) generation is a physical phenomenon leading to a dramatic spectral broadening of laser pulses propagating through a nonlinear medium [28]. Photonic-crystal fibers (PCF) capable of generating supercontinuum emission with unamplified pulses added so much to this generation [29]. They are attractive for study of nonlinear effects, as they can be designed to have very small effective areas, thus increasing the nonlinear

effects. Furthermore, the fiber dispersion can be tuned by scaling the sizes of the fiber structure and the distribution of holes[30].

The chromatic dispersion plays a critical role in SC generation because it determines the extent to which different spectral components of an ultrashort pulse propagate at different phase velocities in the fiber. The importance of dispersion, rather than nonlinearity, in influencing the dynamics of SC generation could be descibed by the experiment reviewed in ref [31] while keeping the peak power and pulse duration at constant value. Three different regimes could be identified according to pumping wavelength.

Normal group-velocity dispersion (GVD) pump wavelength: if the pump wavelength is far from the zero dispersion wavelength (ZDW), the initial dynamics of SC are dominated by the interaction of SPM and normal GVD which gives approximately symmetric temporal and spectral properties. Because this leads to significant temporal broadening and rapid decrease of peak power over the first few centimeters of propagation, the extent of nonlinear spectral broadening is necessarily limited.

Zero dispersion pump wavelength: when the pump pulses are launched close to the zero-dispersion wavelength of the nonlinear media, the propagation of ultrashort pulses in optical fibers near the zero-dispersion wavelength allows for relatively long interaction lengths with high peak intensities, which can result in dramatic nonlinear effects [32].

Anomalous GVD pump wavelength: For pump wavelengths exceeding ZDW, the energy transferred into the anomalous GVD regime increases, and soliton dynamics play an important role. Specifically, the spectral and temporal SC characteristics exhibit signatures of soliton fission. This can lead to instabilities for longer pulses (poor coherence), although the averaged spectra exhibit artificial smoothness.

1.4 Outline of this Thesis

This thesis contains five chapters; Introduction, Theoretical Considerations, Experimental method, Data description and Results, Conclusions.

Chapter 2 is divided into two parts. The first explains the theoretical background of the Chirped Pulse Amplification process while the second covers the light-atom interaction in optical fibers. The first part begins with an overview of the pulse propagation in media. This is followed by a description of the linear and nonlinear impairments that these optical pulses experience due to propagation in optical fiber. It also talks about stretching and

compression of optical pulses by bulk gratings and the compensation of the dispersion orders. The second part presents an overview of light-atom interaction and the amplification process in fibers. It includes the behaviour of Yb-doped fiber amplifiers as a function of the input seed wavelength. It also provide a short description of the drawbacks of optimal amplification in optical fibers, and the considerations for dual-wavelength amplification in a single optical fiber amplifier.

Chapter 3 presents an overview of the previous work done for generating mid-infrared radiation. Following this, a thorough overview of the different parts of this experimental work was presented. This includes the generation of the input broad-bandwidth spectrum by supercontinuum, the structure of the stretcher and compressor used in building the CPA system, and the different amplifier stages inserted and their role in improving the efficiency of the amplifier system. It presents a comparison between different pumping geometries as well as the combination of several fiber amplifier lengths and their effects on the output average power of the system. It also includes a review of the importance of double-clad fibers in amplification.

Chapter 4 presents a thorough overview of the discussion of the results obtained in this experiment.

Chapter 5 presents a conclusion for this thesis and a summary of the key results obtained within the experimental chapter.

Finally, Appendix A presents the computer modeling made for choosing the optimal fiber length required for optimal fiber amplification of the two colors (1035nm & 1105nm) chosen in this work.

Chapter 2

Theoretical Considerations

2.1 Chirped Pulse Amplification

Fiber Chirped Pulse Amplification (CPA) laser systems allow the production of ultra-short high-peak-power pulses in fiber lasers [18]. A laser pulse is firstly generated in an optical resonator. Before amplification, it is frequency chirped and temporally expanded using a fiber [33], or an anti-parallel grating pair with a telescope [19]. The stretched pulse allows more energy to be extracted from the amplifier system than would be by a short pulse. After amplification, the pulse is compressed by a parallel grating pair [20] to a picosecond or a sub-picosecond duration.

It is only possible to stretch and compress the ultrashort optical pulses due to their spectral properties (broad bandwidth) where spectrally dependent spatial effects are taken such as angular dispersion (AD) to generate a time dilation between spectral components.

However in order to understand more deeply the importance of CPA in pulse amplification, it is useful to study threoretically the behaviour of optical pulses when propagating through optical amplifiers.

2.1.1 Optical pulses propagation in single-mode fibers

Dielectric fibers are a form of dielectric waveguides which represent a possible medium for the guided transmission of energy at optical frequencies. Electromagnetic waves are guided along the definable boundary between the regions of different refractive indexes. When optical pulses propagate inside a fiber, the bound electrons regenerating the incoming fields

are driven into harmonic and anharmonic motion which is manifested as complex changes (distortions) in the pulse's shape and spectrum.

Mathematically, the propagation of optical pulses in optical fiber amplifiers is described by the wave equation obtained from Maxwell's equation. It is expressed as [33]:

$$\nabla^2 E\left(r,t\right) - \frac{1}{c^2}\frac{\partial^2 E\left(r,t\right)}{\partial t^2} = \mu_o \frac{\partial^2}{\partial t^2}\left(P_L(r,t) + P_{NL}(r,t)\right) \tag{2.1}$$

P_L, P_{NL} are the linear and the nonlinear parts of the collection of the electric dipole moments (the induced polarization P_{ind} in the medium), and E is the electric field. Eq.(2.1) provides the general formalism for studying the linear and nonlinear effects in optical fibers. The distortion effects of the pulse during the propagation in optical fibers can be studied by further simplifying this equation.

Firstly, by considering a low-intensity optical pulse propagating through the amplifier, the nonlinear polarization $P_{NL}(r,t)$ can be considered as a small perturbation to the total induced polarization in the medium and thus is neglected. Therefore, the fourier transform of Eq.(2.1) can now be written as:

$$\nabla^2 \tilde{E}\left(r,\omega\right) + \varepsilon\left(\omega\right)\frac{\omega^2}{c^2}\tilde{E}\left(r,\omega\right) = 0 \tag{2.2}$$

Since fiber amplifiers are usually used in the wavelength range where silica possess low optical loss, then $\varepsilon\left(\omega\right)$, the dielectric constant, can be replaced by only the linear refractive index $n^2\left(\omega\right)$ (still Low-intensity input signals) and Eq.(2.2) becomes:

$$\nabla^2 \tilde{E}\left(r,\omega\right) + n^2\left(\omega\right)\frac{\omega^2}{c^2}\tilde{E}\left(r,\omega\right) = 0 \tag{2.3}$$

where $\tilde{E}\left(r,\omega\right)$, the complex phasor amplitude, is the Fourier transform of $E(r,t)$.

The change of the amplitude of the wave is measured by a linear propagation constant β. It can be written from Eq.(2.3) as:

$$\beta^2\left(\omega\right) = n^2\left(\omega\right)\frac{\omega^2}{c^2}$$

However, when optical pulses propagate inside a fiber amplifier, both dispersive and nonlinear effects will influence their shape and spectrum. In this case, the nonlinear part

ε_{NL} is now added to $\varepsilon(\omega)$ in Eq.(2.2):

$$\varepsilon(\omega) = n^2(\omega) + \varepsilon_{NL} \tag{2.4}$$

Eq.(2.2) is solved by using the method of separation of variables. The solution is assumed to be of the form

$$\tilde{E}(r, \omega - \omega_o) = F(x, y)\,\tilde{A}(z, \omega - \omega_o)\, exp[i\beta_o z], \tag{2.5}$$

where $F(x, y)$ is the actual modal distribution, $\tilde{A}(z, \omega - \omega_o)$ is a slowly varying function of z containing the transverse amplitude and phase variation of travelling wave and β_o is the wave number. Substituting Eq.(2.5) in Eq.(2.2) leads to two equations for $F(x, y)$ and $\tilde{A}(z, \omega - \omega_o)$[33]:

$$\frac{\partial^2 F}{\partial x^2} + \frac{\partial^2 F}{\partial y^2} + \left[\varepsilon(\omega)\frac{\omega^2}{c^2} - \tilde{\beta}^2\right] F = 0 \tag{2.6}$$

$$2i\beta_o \frac{\partial \tilde{A}}{\partial z} + \left(\tilde{\beta}^2 - \beta_o^2\right)\tilde{A} = 0 \tag{2.7}$$

The wave number $\tilde{\beta}$ is determined by solving the eigenvalue equation (2.6). The dielectric constant $\varepsilon(\omega)$ in Eq.(2.6) is approximated by

$$\varepsilon = (n + \Delta n)^2 \approx n^2 + 2n\Delta n \tag{2.8}$$

where for single mode fibers Δn is a small perturbation given by

$$\Delta n = n_2 |E|^2 \tag{2.9}$$

Eq.(2.6) is solved using first-order perturbation theory. By replacing $\varepsilon(\omega)$ with n^2, the modal distribution $F(x, y)$ and the corresponding wavenumber β are obtained. However, from Eq.(2.6) the eigenvalue is written as:

$$\tilde{\beta}(\omega) = \beta(\omega) + \Delta\beta \tag{2.10}$$

where $\beta(\omega)$ is linear propagation contant, and the last term $\Delta\beta$ includes both fiber loss and nonlinearity.

By replacing the term $\tilde{\beta}^2 - \beta_o^2$ of Eq.(2.7) by $2\beta_o\left(\tilde{\beta} - \beta_o\right)$ and substituting the value

of $\tilde{\beta}(\omega)$ from Eq.(2.10), Eq.(2.7) can be written as

$$\frac{\partial \tilde{A}}{\partial z} = i\left[\beta(\omega) + \Delta\beta - \beta_o\right] \tag{2.11}$$

The physical meaning of this equation provides that each component within the pulse envelope aquires, as it propagates down the fiber, a phase shift whose magnitude is both frequency and intensity dependent [33].

2.1.2 Kerr Effect

Under the influence of intense electromagnetic fields the response of the polarization to an optical excitation in a nonlinear dielectric media becomes nonlinear ($P_{NL}(t) = \chi^{(n)}E^n(t)$; $n \geq 2$), Eq(2.4). This case occurs when short optical pulses characterized with high peak power are being amplified in optical fibers. However, the total polarization induced by electric dipoles is commonly represented by Eq.(2.1). The right hand side corresponds to the different possible responses a material can undergro when being exposed by different signal powers.

Since the glass structure SiO_2 of optical fiber inherently possesses an inversion symmetry, second-order and subsequent higher even-order electrical susceptibilities vanishes [34], leaving the $\chi^{(3)}$ response of the material to be the first nonlinear polarization term which is responsible for four-wave mixing and nonlinear refraction. Therefore, mentioning the nonlinear effects in optical fibers corresponds to some of the common nonlinear $\chi^{(3)}$ processes.

When the intensity of the pulse is high enough to modulate the index of refraction of the material, a nonlinear Kerr effect takes place giving the refractive index as:

$$\tilde{n}(\omega, I) = n(\omega) + n_2 I \tag{2.12}$$

where I is the optical intensity inside the fiber, and n_2 is the nonlinear refractive index coefficient which is a measure of the fiber nonlinearity. The first term is the linear refrective index while the second, Eq.(2.9), is the intensity dependent refractive index. Eq.(2.12), showing that the refractive index is no longer constant but rather a linear function of the intensity, is commonly referred to as the *optical Kerr effect*.

2.1.2.1 B-integral

As the pulse duration of the input pulses decreases from the nanosecond to the picosecond and femtosecond regimes, it becomes increasingly difficult to extract the stored energy from the fiber amplifiers without causing detrimental nonlinear effects. Amplification of these picosecond or femtosecond to a high power levels is not possible because of the intensity dependent refractive index (Optical kerr effect) which produces a nonlinear phase retardation given by:

$$B \equiv \frac{2\pi}{\lambda} \int_0^L n_2(z)\, I(z)\, dz,$$

where L is the length of the fiber amplifier.

The B-integral is defined as a cumulative measure of the nonlinear interaction in the lasing medium of the fiber amplifier. A generally accepted criterian for high-power laser systems is that the cumulative B integral must be kept somewhere below the value $B \leq 3\,to\,5$ to avoid serious nonlinear damage and distortion effects due to self-focusing and self-phase modulation (SPM) ($B \leq 1$). However, using CPA is to keep the intensity level in the lasing medium of the fiber amplifier below a certain B intergral level and thus avoid self-focusing & SPM to take place in fibers.

2.1.2.2 Self-Phase Modulation

Self-phase modulation is a result of the Kerr effect. The intensity dependent refractive index $n_2 |E|^2$, Eqs.(2.9) & (2.12), induces a phase distribution that is proportional to the intensity distribution of the lightwave. For a pulse signal given as: $E(t) = A(t)exp[i\phi_{total}(t)]$, the intensity-dependent temporal phase shift, $\phi_{SPM}(t)$, for the pulsed signal is solved as:

$$\phi_{SPM}(t) = -\left(\frac{2\pi}{\lambda}\right) n_2 \int I(z,t)\, dz \tag{2.13}$$

where $I(z,t)$ is the time dependent pulse intensity. Except for the minus sign, the right hand side of Eq.(2.13) is the B-integral. As the laser pulse experiences a time-varying phase modulation, produced by the intensity variation of the pulse itself, a new frequency chirp generates and adds to the original frequency chirp of the laser pulse. From equation (2.13), the new frequency chirp $\Delta\omega_{SPM}$ can be written as:

$$\Delta\omega_{SPM}(t) = \left(-\frac{\partial\phi_{spm}(t)}{\partial t}\right) = -\left(\frac{2\pi}{\lambda}\right) n_2 \int \frac{\partial I}{\partial t} dz \tag{2.14}$$

The time dependence of $\Delta\omega_{SPM}(t)$ is referred to as frequency chirping. The chirp induced by SPM is proportional to the propagated distance in fiber, i.e. increases in magnitude with the propagated distance. In other word, new frequency components are generated continuously as the pulse propagates down the fiber.

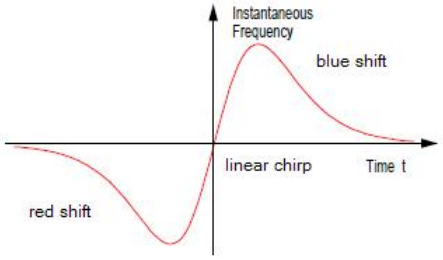

Figure 2.1: Instantaneous frequency of a Gaussian pulse during propagation through a medium with positive selfphase modulation [35].

The temporal variation of the induced chirp $\Delta\omega_{SPM}(t)$ is negative on the leading and falling edges of the pulse and is positive and linear in the central region. Only this central linear chirp can be compensated by a linear dispersion element such as a pair of parallel gratings.

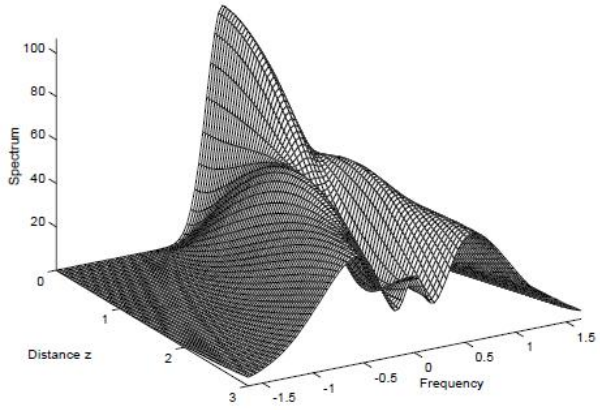

Figure 2.2: Spectrum of a Gaussian pulse subject to self-phase modulation [35].

2.1.3 Dispersion

Linear impairments in optical fibers are those that manifest themselves independently of the signal power, and cannot be avoided simply by ensuring moderate in fiber average and peak powers. They result from the nonlinear dependence of the refractive index $n(\omega)$ and the absorption on the frequency ω of incident electromagnetic (EM) wave. The refraction index can be written in terms of the density of atoms N, the electron charge e and mass m, the oscillator strength f_{vo} of the transition from the atomic ground state o into the excited one v, the frequency $\omega_{vo} = (E_v - E_o)/\hbar$ of this transition, and the width γ_v of the excited state:

$$n(\omega) = 1 + \frac{2\pi N e^2}{m} \sum_v \frac{f_{vo}}{\omega_{vo}^2 - \omega^2 - i\omega_{vo}\gamma_v} \tag{2.15}$$

$n(\omega) - 1$ is nothing but the response of a medium to the incoming electromagnetic wave. The real part of Eq.(2.15) gives the dispersion which optical pulses experience while propagating in optical fibers. This effect is manifested as a temporal spreading of the pulse. The imaginary part gives the absorption of the EM waves. The linear impairments discussed below includes only dispersion as attenuation is negligible due to the short fiber lengths used in amplification.

2.1.3.1 Chromatic Dispersion in single-mode Fibers

Chromatic dispersion (or Group-velocity dispersion) is an important characteristic of an optical fiber. This detrimental effect is characterized by light of different wavelengths experiencing different refractive indices in the optical fiber and, accordingly, the different wavelengths travel at different speeds, $c/n(\omega)$, within the fiber. This generates a frequency dependent phase delay added to the pulses which comes from the propagating term $e^{-i(\beta z - \omega t)}$ in the electric field equation, where $\beta = \omega/v = n\,\omega/c$ is a nonlinear function of the frequency due to the index of refraction n.

By taking the inverse of the propagation equation, Eq.(2.11), the exact functional form of the propagation constant can be derived. However, because the exact form is rarely known [33], it is useful to expand the mode-propagation coefficient $\beta(\omega)$ in a Taylor series which describes the effect of fiber dispersion on a light wave centered at frequency ω_o,

$$\beta(\omega) = \beta_o + (\omega - \omega_o)\beta_1 + \frac{1}{2}(\omega - \omega_o)^2\beta_2 + \frac{1}{6}(\omega - \omega_o)^3\beta_3 + \cdots \tag{2.16}$$

where

$$\beta_m = (\frac{d^m \beta_o}{d\omega^m})_{\omega-\omega_o} (m = 0, 1, 2, \dots).$$

The first four mode-propagation constants are given by

$$\beta_o = n(\omega_o)\frac{\omega_o}{c} \tag{2.17}$$

$$\beta_1 = \frac{1}{c}\left(n + \omega\frac{dn}{d\omega}\right) = \frac{1}{v_g} = \frac{n_g}{c}, \tag{2.18}$$

$$\beta_2 = \frac{1}{c}\left(2\frac{dn}{d\omega} + \omega\frac{d^2n}{d\omega^2}\right) = \frac{d}{d\omega}\left(\frac{1}{v_g}\right) \tag{2.19}$$

$$\beta_3 = \frac{1}{c}\left(3\frac{d^2n}{d\omega^2} + \omega\frac{d^3n}{d\omega^3}\right) = \frac{d^2}{d\omega^2}\left(\frac{1}{v_g}\right) \tag{2.20}$$

The pulse envelope moves at the group velocity $v_g \equiv 1/\beta_1$ (the reciprocal of the group delay per unit length), while the effects of group velocity dispersion (GVD) in broadening pulses are governed by β_2. The parameter β_3 is simply the change in the GVD as a function of the angular frequency ω. Generally, the cubic and higher-order terms are negligible if the spectral width $\Delta\omega \ll \omega_o$. For optical-fibers the GVD is often quantified in terms of signal wavelength rather than frequency. This is defined by the dispersion parameter, D, where

$$D = \frac{d\beta_1}{d\lambda} = -\frac{2\pi}{\lambda^2\beta_2}. \tag{2.21}$$

Either anomalous ($D > 0$, $\beta_2 < 0$) or normal ($D < 0$, $\beta_2 > 0$) dispersion characteristics can be possessed by fibers. β_2, for silica fibers, is positive in the range where the wavelength is less than the resonance value and negative elsewhere. From this parameter one can conclude that shorter wavelengths are more exposed to chromatic dispersion than longer wavelengths. The propagation of an optical pulse, $E_{in}(0,t)$, through a length of fiber, L, generates a quadratic spectral phase (linear chirp), described by:

$$\tilde{E}_{out}(z,\omega) = \tilde{E}_{in}(0,\omega) exp\left[-\frac{i\lambda^2\omega^2 DL}{4\pi c}\right]. \tag{2.22}$$

This equation shows that GVD changes the phase of each spectral component of the

pulse by an amount that depends on both the frequency and the propagated distance.

For a Gaussian pulse, the amplitude at any distance z along the fiber could be given as [33]:

$$E_{out}(z,t) = E_{in}(0,0)\frac{\tau_o}{(\tau_o^2 - i\beta_2 z)^{\frac{1}{2}}} exp\left(-\frac{t^2}{2(t_o^2 - i\beta_2 z)}\right) \tag{2.23}$$

where τ_o is the pulse half-width at $1/e$ intensity point, and t is the retarded time. The quadratic phase term distorts temporal distribution, generally resulting in the broadening of the optical pulse. Despite such phase changes, this does not affect the pulse spectrum.

Because of the time dependence of the phase of the pulse, this implies that the instantaneous frequency differs across the pulse from the central frequency ω_o. The difference $\Delta\omega$ is just the time derivative of the phase.

$$\Delta\omega_L(t) = -\frac{\partial\phi}{\partial t} = \frac{sgn(\beta_2)\,(2z/L_D)}{1 + (z/L_D)^2}\frac{t}{\tau_o^2} \tag{2.24}$$

where $L_D = \tau_o^2/|\beta_2|$ is the dispersion length. Eq.(2.24) shows that the frequency changes linearly across the pulse, i.e., a fiber imposes linear frequency chirp on the pulse. This linear change of frequency is usually dechirped by using a two grating stretcher or compressor system according to the sign of β_2.

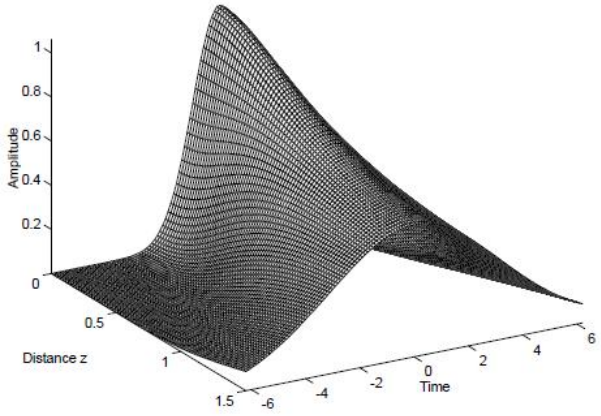

Figure 2.3: Amplitude of the envelope of a Gaussian pulse in a dispersive medium [35].

The compact CPA system built by combining a fiber stretcher and a conventional grating compressor encountered a main difficulty when recompressing the chirped amplified pulses.

This is due to the mismatch of all dispersion orders between a fiber or a fiber grating stretcher and a diffraction grating compressor which prevented from achieving a bandwidth-limited femtosecond pulses duration [36]. The SOD of a material which can be derived from Eq.(2.40) is given as:

$$\frac{d^2\Phi^{(mat)}}{d\omega^2} = \frac{\lambda_o^3 l_{(mat)}}{2\pi c^2}\frac{d^2n}{d\lambda^2}\,|_{\lambda_o}, \tag{2.25}$$

while the TOD is defined as:

$$\frac{d^3\Phi^{(mat)}}{d\omega^3} = -\left(\frac{\lambda_o^4}{4\pi c^3}\frac{d^2n}{d\lambda^2}\,|_{\lambda_o} + \frac{\lambda_o^5}{2\pi^2 c^3}\frac{d^3n}{d\lambda^3}\,|_{\lambda_o}\right) l_{(mat)} \tag{2.26}$$

2.1.3.2 Parallel Gratings

In order to compensate the linear frequency chirp generated as the pulse emerges a transparent medium, a parallel grating system is generally used. The grating system produces a spectral phase delay opposite to that formed by dispersive medium.

In the time domain, the complex amplitude of the electric field of an optical pulse is given as:

$$E_o(t) = A(t).exp[i\phi(t)] \tag{2.27}$$

where $A(t)$ is the complex envelope and $\phi(t)$ is the phase.

A chirped Gaussian pulse incident into a grating pair compressor can be written as [37]:

$$E_o(t) = A(t)\ .exp\left\{i\left[\frac{1}{2}b\left(\frac{t}{T}\right)^2 + \phi_{NL}(t)\right]\right\} \tag{2.28}$$

$$= A\,exp\left[-\frac{1}{2}\left(\frac{t}{T}\right)^2\right].exp\left\{i\left[\frac{1}{2}b\left(\frac{t}{T}\right)^2 + \phi_{NL}(t)\right]\right\} \tag{2.29}$$

The first part of the product represent the initial unchirped pulse while the second represents both the linear and the nonlinear frequency chirped. T is the half pulsewidth at e^{-1} intensity point, $b \approx \Delta\omega_L(t)T/2$ defines the amount of linear chirp, and $\phi_{NL}(t)$ represents the possible nonlinear frequency chirp ($\phi_{NL} = O(t/T)^3$) generated from the optical fiber or expansion gratings.

The frequency chirp of the input optical pulse is the time derivative of the initial phase

variation:

$$\frac{\partial\phi(t)}{\partial t} = bt/T^2 + \frac{\partial\phi_{NL}(t)}{\partial t} \tag{2.30}$$

The second term results in a large phase shifting which distorts the compressed pulse shape and forms a low perturbation frequency disturbance known as pedestals (imperfectly compressed pulses carrying significat amount of energy) which lower the peak intensity of the main compressed pulse. This phase modulation can be compensated by adjusting the angle (nonlinear chirp from orientational mismatch between gratings of the system) of the compression gratings. The first term is a small linear phase shifting which can be normally compensated by adjusting the grating separation distance (linear chirp) in a CPA system.

However, in order to explain the CPA system, it is useful to express the electric field in the Fourier domain. Eq.(2.27) is written as:

$$E_o(\omega) = A(\omega).exp[i\phi(\omega)] \tag{2.31}$$

where $\phi(\omega)$ is the spectral phase. For a Gaussian pulse the electric field in the fourier domain can be written as [37]:

$$E_o\left(\omega^{'}\right) = exp\left[-i\frac{\omega^{'2}T^2}{2b}\right].\int A(t)exp\left[i\frac{b}{2}\left(\frac{t}{T} - \frac{\omega^{'}T}{b}\right)^2\right]dt \tag{2.32}$$

where $\omega^{'} = \omega - \omega_o$

The integral in the RHS is an approximation commonly used in diffraction theory. Compression of pulses with a large frequency chirp is performed by using a pair of gratings to eliminate the phase term $exp\left[-i\frac{\omega^{'2}T^2}{2b}\right]$.

It is only possible to dechirp ultrashort pulses because of the spectral properties of these pulses; they have broadband spectral width. The relation between spectral width and the wavelength bandwidth is formulated as:

$$\Delta\omega = 2\pi\Delta\nu = \frac{2\pi c}{\lambda_o^2\triangle\lambda} \tag{2.33}$$

where the speed of light is c, λ_o is the central pulse wavelength and $\Delta\lambda$ is the pulse bandwidth. The enormous broad bandwidth of ultrashort pulse makes it possible to take the advantage of angular dispersion (AD) in compressing these pulses. By using the appro-

priate arrangement of the diffraction-grating in compression, the components of different wavelengths $\lambda_1$and λ_2 incident into a grating element will diffract at different angles, and thus will experience different time delays at the output of the grating system.

Conventional grating CPA system are so useful in compensating the orders of dispersion. The main properties of this systems are understood easily by referring to Fig.(2.4). The first gratnig diffracts the input beam with wave vector k_{in} and input path vector l into the direction k_{out}. The beam passes between the first and the second gratings and is diffracted back into its original direction. The phase difference by the diffracted beam and the reference beam is: $\Phi(\omega) = k_{out}.l$.

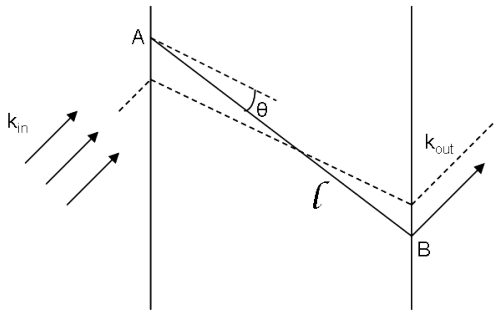

Figure 2.4: A parallel grating pair structure. The path of the central beam is shown by a dashed line. The path of other beam components is shown as l .

After passing the first grating, the beam is diffracted into a frequency-dependent angle $\theta_r(\omega)$ which is governed by the grating law. In the case of first-order diffraction it is given by:

$$2\pi c/\omega = d\left[sin\theta_r(\omega) - sin\theta_i\right] \tag{2.34}$$

where d is the groove spacing of the grating, θ_i is the angle between the incident wave vector and the normal to the first element; $\theta_r(\omega)$ is the angle of the outgoing wave vector, which is a function of frequency. In other words, the blue path of an optical spectrum, diffracted by a grating, is shorter than the red one, and results in a time delay ($\tau = \frac{\partial\Phi}{\partial\omega}$) that is an increasing function of the wavelength. Therefore, an initial Fourier Transform limited pulse will exit a pair of gratings with a chirp and a much longer duration [20].

A single pass through the grating pair produces a spatially chirped beam, and a mirror is generally used to double the pass through grating pair which double the dispersion introduced by the system but negates the spatial chirp. The spectral phase introduced by

Treacy's pair of gratings is given by the equation:

$$\Phi(\omega) = 2\frac{\omega}{c}\left(\frac{l_{(cmp)}}{cos\theta_i}\right) cos\left(\theta_i - \theta_r(\omega)\right) \tag{2.35}$$

where $l_{(cmp)}$ is the slant distance of the gratings, θ_i and θ_r are the incident and diffracted angles, respectively.

The spectral frequency-dependent phase shift [Eq.(2.35)] imparted by a dispersive device (a stretcher, a compressor, or a material) can be expressed in a Taylor expansion about a central frequency ω_o:

$$\Phi(\omega) = \Phi(\omega_o) + \Phi_1(\omega - \omega_o) + \Phi_2(\omega - \omega_o)^2 + \Phi_3(\omega - \omega_o)^3 + ... \tag{2.36}$$

Φ_1 is the group delay of the pulse, and Φ_2 , Φ_3 are, respectively, the second- and third-order dispersion terms. For a parallel grating pair system, the second derivative of the phase (group velocity dispersion) is given as [38]:

$$\frac{d^2\Phi^{(cmp)}(\omega)}{d\omega^2} = -\frac{\lambda_o^3 l_{(cmp)}}{4\pi c^2 d^2\left\{1 - \left[\lambda_o/d - sin\,\theta_i^{(cmp)}\right]^2\right\}} \tag{2.37}$$

where $l_{(cmp)}$ is the slant separation distance of the gratings, λ_o is the central wavelength, d is the groove spacing, c is the speed of light and θ_i is the angle of incidence. This equation shows that the GVD is not perfectly linear with wavelength. It depends on the angle of incidence to the system, the groove density of the grating, and increases linearly with the distance between gratings. It also shows that grating pairs always exhibit a negative dispersion which makes it possible to chirp a short pulse or to compress a positively chirped pulse.

The third order dispersion (TOD) is given as:

$$\frac{d^3\Phi^{(cmp)}(\omega)}{d\omega^3} = -\Phi_2^{(cmp)}\frac{\lambda_o}{2\pi c} \times \left\{1 + \frac{\lambda_o}{d}\frac{\lambda_o/d - sin\,\theta_i^{(cmp)}}{1 - \left[\lambda_o/d - sin\,\theta_i^{(cmp)}\right]^2}\right\} \tag{2.38}$$

It is important to note and conclude from these two equations, that in chirped pulse amplification systems the higher the stretching factor, i.e. larger $l_{(cmp)}$, the harder it is to achieve perfect recompression.

Compressing a pulse of tens of femtosecond in duration means that the final residual

group delay of the pulse must be almost constant over all the ultrabroad pulse bandwidth. Under these conditions, the higher order terms can become significant, which would leave the resulting compressed pulse with non-linear phase distortion.

2.1.3.3 Telescope

Because the parallel grating system will always negatively chirp input pulses, Eq. (2.37), another system (known as stretcher) of opposite dispersion sign is required to obtain a diffraction limited pulse.

Martinez [19] realized that placing a 1:1 telescope inside a parallel grating system changes the sign of the chirp introduced by the compressor. The positive compressor (Stretcher) proposed was of different setting and perfectly matching to all orders of the negative dispersion grating pair.

In order to build the stretcher, a magnification telescope consists of two thin lenses of focal distances f_1 and f_2, with a distance $f_1 + f_2$ between each one is introduced between two gratings. The gratings are placed anti-parallel to each other at a distance l, as if they were a reflection of each other.

When inserting a telescope between the two gratings, the effective length that frequency components will undergo is given as [19]:

$$l_{eff} = \left[l - 2\left(f_1 + f_2\right)\right]\left(f_1/f_2\right)^2 \tag{2.39}$$

this value can be positive or negative depending on the position of the two gratings with respect to the focal length of the telescope lenses. This corresponds to a change in the GVD sign which by turn leads to a postive or negative chirp pulses.

This can simply explained by writing the second order disperison in terms of the path length P ($P = l\,cos\,\theta_r$):

$$\frac{d^2\Phi}{d\omega^2} = \frac{\lambda^3}{2\pi c^2}\frac{d^2P}{d\lambda^2} \tag{2.40}$$

For a grating system, Eq. (2.40) can be written as [38]:

$$\frac{d^2\Phi^{(str)}\left(\omega\right)}{d\omega^2} = \frac{\lambda_o^3 l_{(str)}}{4\pi c^2 d^2\left\{1 - \left[\lambda_o/d - sin\,\theta_i^{(str)}\right]^2\right\}} \tag{2.41}$$

while the third order is written as:

$$\frac{d^3\Phi^{(str)}(\omega)}{d\omega^3} = -\Phi_2^{(str)}\frac{\lambda_o}{2\pi c}\times\left\{1+\frac{\lambda_o}{d}\frac{\lambda_o/d - sin\,\theta_i^{(str)}}{1-\left[\lambda_o/d - sin\,\theta_i^{(str)}\right]^2}\right\} \tag{2.42}$$

where $l_{(str)}$ is the effective length of dispersion. Therefore, the angular dispersion can be either positive or negative manifesting this as positively or negatively linear chirp pulses.

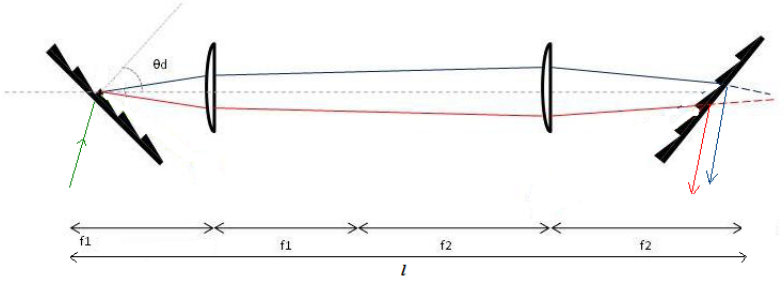

Figure 2.5: A stretcher schematic. The telescope changes the dispersion sign, leading to a positive chirp

2.1.3.4 Difference between ratio of dispersion orders in fibers & grating pairs

In order for the CPA system to work properly, i.e. to stretch, amplify, and compress a pulse to its transform limit, it is necessary to compensate simultaneously the second-order dispersion (SOD) and the third-order dispersion (TOD). In a conventional CPA system the compressor can be made to impart the correct amount of SOD and TOD by adjustment of the two obvious degrees of freedom of a grating pair: the incidence angle at the gratings, and the separation of the gratings. If the incidence angle at the gratings is not set to the correct value, adjustment of the grating separation will only fully compensate the SOD, leaving TOD and, consequently, a poorly compressed pulse.

Equations (2.37, 2.38) shows that both compressor and stretcher exhibit a SOD and TOD of opposite signs. Therefore, a good pulse compression can be expressed in terms of the absolute values as:

$$|\Phi_2|^{(cmp)} = |\Phi_2|^{(str)} + |\Phi_2|^{(mat)}, \tag{2.43}$$

$$|\Phi_3|^{(cmp)} = |\Phi_3|^{(str)} - |\Phi_3|^{(mat)}. \tag{2.44}$$

since the SOD and the TOD of the material is proportional to the length of the material, then the two equations can be written as:

$$|\Phi_2|^{(cmp)} = |\Phi_2|^{(str)} + |\beta_2|\, l_{(mat)} \tag{2.45}$$

$$|\Phi_3|^{(cmp)} = |\Phi_3|^{(str)} - |\beta_3|\, l_{(mat)} \tag{2.46}$$

From these equations, it is shown that the angle of incidence of the compressor is a function of the fiber amplifier length. Therefore, as the fiber length changes the angle of incidence must be changed to retain the SOD and TOD compensation. The difficulties in the alignment of the system is clear from the signs of the CPA system devices. They are different for both stretcher and compressor while are the same for the amplifier. In other word, TOD to GVD ratio introduced by the YDFA has an opposite sign to that introduced by a grating pair compressor. This means that if the compressor is set to perfectly compensate the GVD, the TOD of both the YDFA and the compressor will simply add, resulting in significant pulse broadening and pulse shape distortion.

2.2 Two Colour Amplification in Yb:fiber Amplifier

Fiber amplifiers are optical amplifiers based on optical fibers as gain media. The optical fiber simply comprises layers of different refractive indexes in order to guide optical lasers along it. Nowadays, fibers are available in different layer structures, yet all this is for better guidance and better performance. However, all these fibers have a common layer, known as the fiber core. This layer has the highest refractive index surrounded by another of lower refractive index. The cores are usually doped with rare-earth materials to act as the gain medium of optical fiber amplifiers. They can be doped with different rare earth ions such as Erbium, Neodymium, Ytterbium, Praseodymium, or Thulium. Doped ions in the fiber cores are usually selected based on the range of wavelengths needed to be amplified, and thus dopants of gain profile peaking at the input signal. For example, to amplify near-IR light in 1-1.1 μm region [15], ytterbium doped fiber (YDF) amplifiers are preferred as they have absorption bandwidths extending from 800 to 1064nm and emission bandwidths extending 970nm to 1200nm.

The behavior of a fiber amplifier is determined by the absorption and emission cross sections of dopant which can vary according to wavelength and dopant used.

The dependence of the Yb^{3+} ion cross sections on wavelengths is presented in Fig(1) of R. Pachotta et. al. paper[39]. According to this figure, the Yb^{3+} ion has a broad gain profile, yet it overlaps a broad absorption profile. This overlaping is a major drawback for amplifying optical spectrum having a wavelength range from 975 up to 1030 nm. To overcome this, a comprehensive understanding of the operating characteristics of Yb^{3+} fiber amplifier is necessary for building an efficient amplifier system.

2.2.1 Rate Equations for Laser Gain

The interaction between light and atoms is essential for the construction of fiber amplifiers. Atoms are composed from quantized energy levels. Several interactions can take place when the energy difference of two levels ($E = E_2 - E_1$) matches the energy of a photon ($E = hv$) in the system. It is possible that the atom absorbs a photon and, in the process, excites to a higher energy state from E_1 to E_2. Excited electrons will not stay at the excited level for long time before it will eventually drop back down into a lower level in a time known as the lifetime. By doing so, it will emit a photon of radiation in a process called *spontaneous emission* with an energy corresponding to the energy difference between the upper state and the new lower state.

If however, the atom is already in a high-energy state, and a photon of the correct wavelength comes along, it can stimulate the excited atom to emit a photon of exactly the same wavelength and phase as the incident photon, leaving two photons exiting this process going in exactly the same direction. This process is known as *stimulated emission*, and is the basis upon which fiber amplifiers operate.

For light amplification in fibers, two laser sources are needed: one for atoms to be continually excited to their upper states, called the pump, and a second to stimulate atoms, known as the seed. The atoms in a fiber will then emit a light at the seed energy which adds coherently to the seed laser, and thus amplify it. The spontaneous transition in a volume V is frequency dependent and has a rate, probability per unit time, given by:

$$p_{sp} = \frac{d}{V}\sigma(v) \tag{2.47}$$

where $\sigma(v)$ is the cross section of the transition [39]. This transition is independent on photon number from an incident electromagnetic (EM) field but is frequency dependent. Conversely, the probability per unit time for absorption and stimulated emission in a two level system is given by

$$W = p_a = p_s = \eta \frac{d}{V} \sigma(v) \tag{2.48}$$

and does depend on the number of photons (η). The rate of the atom absorbing one photon, or being stimulated to emit one coherently is enhanced by the presence of large number of photons in the incident EM field.

For a two level system, the number of photons per unit area per unit time, or the photon-flux density is defined as:

$$\phi = \frac{I}{hv} \tag{2.49}$$

This equation can be used with the expression of the number of photons per unit area per unit time $\eta = \phi A = \phi \frac{V}{d}$ in a cylindrical volume $V = dA$ of base-area A and the height d to derive a new expression for the probability of a transition.

$$W = \phi \sigma(v) = \frac{I \sigma(v)}{hv} \tag{2.50}$$

where I is the intensity of the incident photon stream, and hv the energy of a single photon in the stream.

In order to obtain the number of photons gained in a medium per unit time per unit volume, it is necessary to know the probability for a photon to be absorbed or to stimulate emission in the amplifier gain medium [40]. If N_1 and N_2 represents the number of atoms per unit volume occupying level one and two, respectively, and the average probability is W, then the average density of absorbed photons and that created by stimulated emission is $N_1 W$ and $N_2 W$, respectively.

If the population difference, $N = N_2 - N_1$, is positive, then the system is in a state of population inversion and the medium act as an amplifier. The photon density gained would simply be NW photons per unit time per unit volume. In the amplifier system, the new photons produced by stimulated emission will move in the same direction as the seed beam and add to the flux ϕ of the system moving in the z direction. The change in flux per unit length in a cylindrical amplifier system is given by,

$$\frac{d\phi}{dz} = NW \tag{2.51}$$

or can be written as differential equation in z by substituting (2.50) in (2.51) to have:

$$\frac{d\phi}{dz} = \gamma(v)\,\phi(v) \tag{2.52}$$

where $\gamma(v) = N\sigma(v)$ is the gain coefficient which represents the net gain in the photon-flux density as well as that in the intensity per unit length of the medium.

The solution of the differential equation is an exponential increasing function of the constant flux $\phi(0)$ designated to be the beginning of the interaction region.

$$\phi(z) = \phi(0)\,exp\left[\gamma(v)\,z\right] \tag{2.53}$$

The total gain $G(v)$ of an amplifier system of interaction length $z = L$ would be the ratio of flux at the beginning of the interaction region to the flux at the end of the region.

$$G(v) = exp[\gamma(v)L]. \tag{2.54}$$

Eq.(2.54) shows that gain increases exponentially as the wave travels down the tube and depends on the population densities of each energy level.

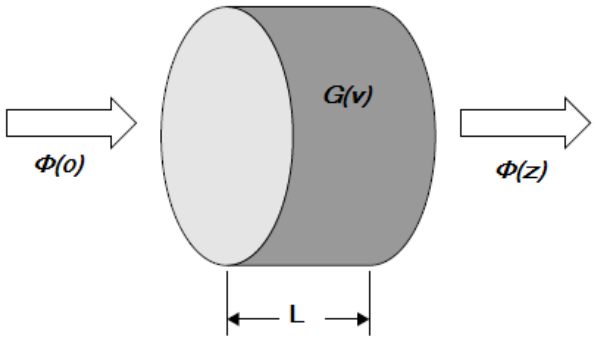

Figure 2.6: Gain in a laser medium

To study the behavior of the gain, rate equations are being used to examine the ways in which the populations change over time. These equations can accommodate all the transitions inherent in amplifiers including pumping, spontaneous and stimulated emission, and absorption.

However, to have gain in a laser system, more energy levels than what a two level system contains must be involved in the pumping and emission process. Generally, most practical

lasers feature a three- and four-level atomic system. They are classed as three- or four-level lasers according to the number of energy levels involved in the actual lasing process.

2.2.1.1 Three Level System

The three level laser system is schematically presented in Fig(2.7). The figure shows a three energy level (involved in a three level laser) ordered from the highest- to the lowest- energy level as: the pump level (level 3), upper lasing level (level 2), and the ground level (level 1). When energy is injected to the gain medium of such a system, atoms are excited from level 1 up to level 3. After being excited, atoms decay quickly to level 2 due to the very short lifetime of the pump level. This decay usually occurs by emitting heat, not photons. Conversely, the upper lasing level has a long lifetime, and so population builds in that level.

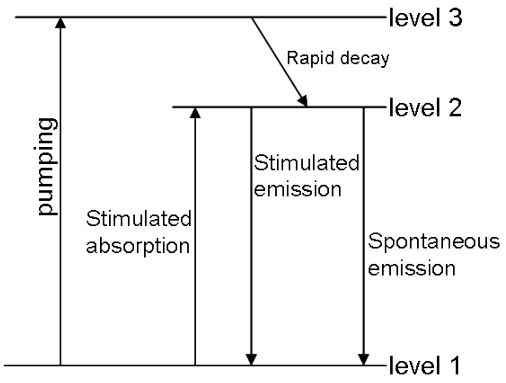

Figure 2.7: Energy level diagraim for a three-level laser system

In a three level laser system, the rate of change of population at different energy states will depend on different processes. In the first, an incoming photon to the gain medium of this type of laser system, excites the atomic system from a lower energy state into a higher energy state; level 1 to level 2. This is called absorption. It is called stimulated absorptions because of the fact that the atoms absorb the incident energy at certain frequencies only. Stimulated absorption occurs when a photon strikes an atom with just exactly the proper energy to induce an electronic transition between two energy states. In the absence of an electromagnetic field, the excited atoms will spontaneously decay after a period of time known as spontaneous lifetime. In case of spontaneous emission of a photon, the probability of its emission is inversely related to the average length of time that an atom can reside in the upper level of the transition before it relaxes. The shorter the spontaneous lifetime,

the greater is the probability that spontaneous emission will occur. Level 2, which has the spontaneous lifetime are know as metastable level. However, the excited atoms will also lose their energy not only by spontaneous emission, but also by induced or stimulated emission and therefore the emission output of the system consists of spontaneous and stimulated emissions. The probability of stimulated emission is proportional to the intensity of the energy density of external radiation unlike the spontaneous emission which depends only on the population of the high energy state; level 2.

Since these transitions are dependent on the rate at which atoms populate each level, it is useful to apply the rate equations in order to analyze the behaviour of this system in emitting laser light. These equations express the rate as a change of population of atoms in each of the three levels.

The process by which atoms are raised from level 1 to level 3 is known as pumping. Considering that the relaxation of the population from the pump level to the upper laser level proceeds very rapidly, an approximation can be made $N_3 \approx 0$ for the populations of the pump level. Under this condition, it is only to deal with two levels in this three level system; level 1 and 2. In this case, the upper pump level is considered empty, and the rate at which the upper laser level becomes populated by the pumping can be written as: $\left(\frac{dN_2}{dt}\right)_p = W_p N_g$. W_p is the rate of absorption, and N_g is the population of the ground level.

The rate at which transitions $2 \rightarrow 1$ occur as a result of spontaneous emission can be written as:

$$\left(\frac{dN_2}{dt}\right)_{sp} = -AN_2 \tag{2.55}$$

where A is the rate of spontaneous emission or the Einstein A coefficient, N_2 is the population of level 2. It can be written as the inverse of the spontaneous emission lifetime, $A = 1/\tau_{sp}$. For stimulated transitions (either emission or absorption) the rates can be written as following:

$$\left(\frac{dN_2}{dt}\right)_{st} = -W_{21}N_2 \tag{2.56}$$

$$\left(\frac{dN_2}{dt}\right)_{ab} = W_{12}N_1 \tag{2.57}$$

The rate of change of population of atoms in the upper lasing level (ULL) is given as:

$$\frac{dN_2}{dt} = W_p N_g + W_{12} N_g - W_{21} N_2 - \frac{N_2}{\tau_{sp}} \tag{2.58}$$

The first term refers to the flow of energy from the ground level to the ULL while the second gives the rate of population increase due to stimulated absorption, the third is the rate of population decrease resulted from stimulated emission, and the last term is the rate of decrease of population due to the spontaneous radiative transtion from level 2 to level 1.

For the ground level, the rate of change of atoms is:

$$\frac{dN_1}{dt} = -W_p N_g - W_{12} N_g + W_{21} N_2 + \frac{N_2}{\tau_{sp}} \tag{2.59}$$

This equation is the same as Eq.(2.58) but of opposite signs. As the stimulated transitions rate W is in fact proportional to the square of the magnitude of the electric field of the em wave, can also be taken as proportional to ϕ. depend on the intensity of the electromagnetic field, The second and the third term in Eqs.(2.58&2.59) account for stimulated transition can be written as: $B_{12}\phi N_1$& $B_{21}\phi N_2$, respectively. The B coefficient is referred to as the stimulated transition per photon, per mode.

2.2.1.2 Four Level System

Four-level systems feature a discrete lower lasing level (LLL) between the upper and the ground energy states other than the mentioned levels of the three-level laser system. In a four level laser , the material is pumped to level 3, which is a fast decaying level, and the atoms decay rapidly to level 2, which is a metastable level. The radiative transitions, the spontaneous and stimulated, takes place from level 2 to level 1 from where the atoms decay rapidly back to level 0, or the ground level. Under this conditions, an approximation can be made $N_1 = N_3 \approx 0$ for populations of level 1 and level 3. Four-level lasers is an improvement on a system based on three level systems. In this case, the laser transition takes place between the second and first excited states. Since lower laser level 1 is a fast decaying level which ensures that it rapidly gets empty and as such always supports the population inversion condition. For this reason, it is much easier to have a population inversion in this laser systen than the three level system.

As mentioned previously in the three level laser system section, if the upper level is considered empty, level 3, the rate at which the upper laser level becomes populated by the pumping, $\left(\frac{dN_2}{dt}\right)_p$, can in general be written as $\left(\frac{dN_2}{dt}\right)_p = W_p N_g$. However, for most

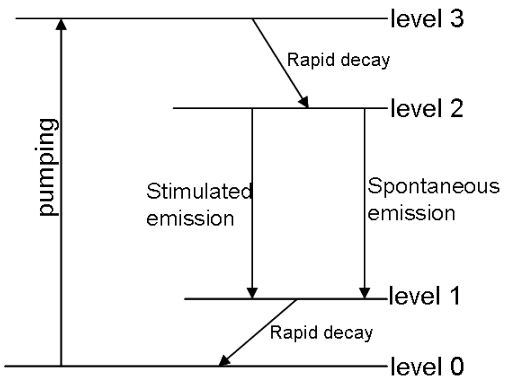

Figure 2.8: Energy level diagram for a four-level laser system.

four-level lasers, the depletion of the ground level, due to the pumping process, can be neglected. With $N_g = const$, the previous equation can then be written more simply as:

$$\left(\frac{dN_2}{dt}\right)_p = R_p \tag{2.60}$$

where R_p is called the pump rate per unit volum or, the pump rate.

The rate of change of population in level 3 is given as:

$$\frac{dN_2}{dt} = R_p - B\phi N - \frac{N_2}{\tau_{sp}} \tag{2.61}$$

The second term gives the rate of population decrease due to the stimulated transition from level 2 to level 1. The last term accounts for the spontaneous transition from level 2 to level 1. As populations in level 1 rapidly decay into level 1, stimulated absorption is not included in this equation. In other words, there is no significant reabsorption of signals during their propagation in materials that behave as four-level laser system.

2.2.2 Amplification in Ytterbium Fiber

Ytterbium doped fiber amplifier must be treated somewhat differently from the treatment of an ideal two level system. In the two level system, no two levels are degenerate (have the same energy), and the same transition cross section can be used to describe both absorption and stimulated emission in some special cases. For ytterbium ion (Yb^{3+}), the levels are actually bands of levels [39], Fig.(2.9), called manifolds. Yb^{3+} exhibits only a ground state

($^2F_{7/2}$ manifold) and a metastable state (so-called because it has a relatively long lifetime, making it almost stable), $^2F_{5/2}$, spaced by approximately 10,000 cm-1[40].

Due to the fact that the pump level of this ion is the metastable state itself, this increases the gain efficiency of this ionic material as there is no downward decay (waisting energy as heat) from the top level (pump level) into the metastabe state (ULL) as a three-level laser exhibits. Besides, the absence of higher energy levels greatly precludes the excited state absorption (ESA) that lower the efficiency of pump absorption. Furthermore, the large band-gap of this ion also precludes the multi-phonon emission (non-radiative decay). These combined features of ytterbium allow for a very strong pump absorption, and thus facilitate the development of high-power fiber lasers.

However, $^2F_{5/2}$ manifold (metastable state) is composed from three sublevels which behaves as the pump levels of this ion. Having these three pump levels, Yb^{3+} can absorb energy at a variety of wavelengths (approximately from 850 to 1070). Therefore, a choice of pump laser sources can be included for pumping Yb^{3+} such as Titanium sapphire (Ti:sapphire) lasers. Besides, the lower manifold (ground level) has four sublevels which can all accept optical transitions from the pump levels. This stretches the emission band of ytterbium for hundered of nanometers (from 970 to 1200).

Fig.(2.9) shows the relevant energy level structure of $Yb^{3+}$and gives a closer discussion of the spectral properties of these fibers. It can be seen from this figure that very different transitions can take place between the two band levels. The transitions between the lowest sub-levels (a and e) correspond to the strong absorption and emission at 975 nm of R. Pachotta fig.(1)[39]. There is also a secondary peak in absorption at 915nm in this figure includes transitions from level a to f and g in Fig.(2.9) while at longer wavelengths a weak shoulder in the absorption spectrum corresponding to a much smaller population at level b. The less population in level b is due to the fact that only 6 % relative to the population of level a are thermally excited into level b at room temperature as calculated from Boltzmann factor. Nevertheless, the thermally excited population plays a significant role in the signal re-absorption loss of the shorter wavelengths beams as they propagate down the fiber. This re-absorption reduces the gain and additionally shifts the gain maximum to longer wavelengths which by raises the threshold for lasing at wavelengths within the dip in the emission spectrum.

The downward lasing decay between the lowest sublevels is for the laser action at the 975nm. Since this emission is a transition between a metastable level (ULL) and a ground level, Fig.(2.7), ytterbium acts as a truly three-level laser system in character. In addition

to this emission into the lowest Stark level (a), other transitions can occur from level e to b, c, and d which correspond to the second peak at 1030nm in the emission spectrum of R. Pachotta et. al. figure[39] with its tail extending out to 1200 nm. The laser action on these transitions (above 1030nm) becomes nearly four level in character, as the emission is into essentially empty levels c and d.

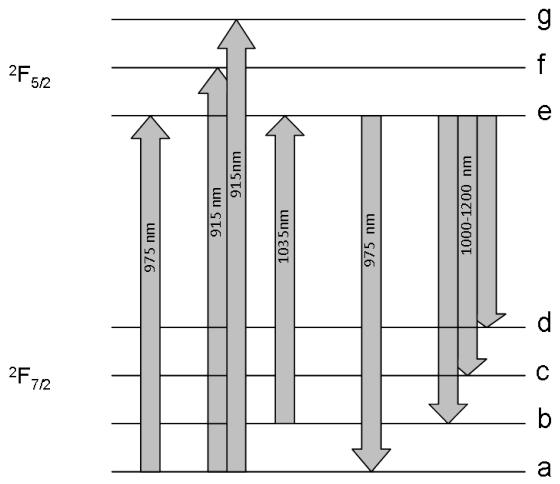

Figure 2.9: The Yb^{3+} energy level structure consisting of 2 manifolds, the ground manifold $^2F_{7/2}$ with 4 stark levels (labeled (a)-(d)) and the excited state manifold labeled $^2F_{5/2}$ with 3 stark levels (labeled (e)-(g)). The approximate energy in wave numbers are indicated above the ground state.

However, by analyzing both the absorption and emission transitions from Figures (R. Pachotta fig.(1)[39] & 2.9), we can conclude that for a fiber amplifier system with many energy levels for the dopant, absorption cross section $\sigma_a(v)$ and emission cross section $\sigma_e(v)$ must be considered for calculating the probability density transition rather than considering them equal as was mentioned before in Eq.(2.50) in the two level system. The rate equations also must be re-written by inserting these cross-section quantities [41]. For the doped-fiber system, the probabilities to undergo absorption and spontaneous emission can now be written as,

$$W_a = \phi\,\sigma_a(v) \tag{2.62}$$

$$W_e = \phi\,\sigma_e(v) \tag{2.63}$$

This leads to a gain coefficient expressed as,

$$\gamma(v) = N_2\sigma_e(v) - N_1\sigma_a(v) \tag{2.64}$$

This equation shows the wavelength-dependence of the ytterbium ion fiber laser action, and therefore, fiber amplifier systems doped with these ions can act as a three or a four level laser system in character depending on the wavelength of amplification.

Due to the dependence of the absorption and emission rate on the number of incident photon to the medium, the intensity of the incoming EM field, Eq.(2.49), it is useful to express the photon flux in terms of the intensities of the seed and pump beams I_s and I_p, Eq.(2.50). In this way the rate equations of the two level system can be rewritten for a general amplifier system to apply to a three level fiber amplifier system [42].

$$\frac{dN_1}{dt} = -\frac{\sigma_{pa}I_p}{hv_p}N_1 - \frac{\sigma_{sa}I_s}{hv_s}N_1 + \frac{\sigma_{se}I_s}{hv_s}N_2 + \frac{N_2}{t_{sp}} \tag{2.65}$$

$$\frac{dN_2}{dt} = \frac{\sigma_{pa}I_p}{hv_p}N_1 + \frac{\sigma_{sa}I_s}{hv_s}N_1 - \frac{\sigma_{se}I_s}{hv_s}N_2 - \frac{N_2}{t_{sp}} \tag{2.66}$$

Equations (2.65, 2.66) describe the general amplifier by using the absorption and emission cross sections for the pump and seed beams, along with the intensities of each beam. These equations are totally analogous with the rate equations of the three and four level system . Under the steady state conditions the solution of these equations can be obtained, and the gain coefficient in (2.64) becomes:

$$\gamma(r,z,v) = \frac{\sigma_s^{'}I_p^{'}(r,z) - 1}{1 + I_s^{'}(r,z) + I_p^{'}(r,z)}N_o \tag{2.67}$$

the new variable $\sigma_s^{'}$, $I_p^{'}$, $I_s^{'}$are defined as:

$$\sigma_s^{'} = \frac{\sigma_{se}}{\sigma_{sa}} \tag{2.68}$$

$$I_p^{'} = \frac{I_p\sigma_{pa}t_{sp}}{hv_s} \tag{2.69}$$

$$I_s^{'} = \frac{I_s(\sigma_{sa} + \sigma_{se})t_{sp}}{hv_s} \tag{2.70}$$

The labels (s, p, sp, se, sa, pa) corresponds to stimulated emission, pumping, spontaneous emission, signal emission, signal absorption, pumping absorption, respectively.

Because the intensities of the seed and pump beams I_s and I_p are dependent on v, z and r, the gain coefficient is dependent on these quantities as well, Eq.(2.67). Its dependence on z is a consequence of the absorption and emission processes inside the fiber. The pump is generally absorbed along the length of the fiber, while the seed power can grow or shrink depending on the gain. To optimize the performance of the fiber amplifier under the constraint that the signal is amplified while having minimum possible ASE, simulations are usually conducted. The differential equation for the length dependence of the seed and spontaneous emission wavelengths are given as [14]

$$\pm\frac{dP_s^{\pm}\left(\lambda_k^s\right)}{dz} = \Gamma\left[\sigma_e\left(\lambda_k^s\right)N_2 - \sigma_a\left(\lambda_k^s\right)N_1\right]P_s^{\pm}\left(\lambda_k^s\right) - \alpha P_s^{\pm}\left(\lambda_k^s\right) \tag{2.71}$$

$$\pm\frac{dP_{ase}^{\pm}\left(\lambda_l^{ase}\right)}{dz} = \Gamma\left[\sigma_e\left(\lambda_l^{ase}\right)N_2 - \sigma_a\left(\lambda_l^{ase}\right)N_1\right]P_{ase}^{\pm}\left(\lambda_l^{ase}\right)$$

$$-\alpha P_{ase}^{\pm}\left(\lambda_l^{ase}\right) + \sigma_e\left(\lambda_l^{ase}\right)N_2\frac{2hc^2\Delta\lambda}{\left[\lambda_l^{ase}\right]^3} \tag{2.72}$$

and the differential equation for the length dependence of the pump is

$$\frac{dP_p\left(\lambda_j^p\right)}{dz} = \Gamma\left[\sigma_e\left(\lambda_j^p\right)N_2 - \sigma_a\left(\lambda_j^p\right)N_1\right]P_p\left(\lambda_j^p\right) - \alpha P_p\left(\lambda_j^p\right) \tag{2.73}$$

The powers of the seed and pump lasers are characterized by Ps, & Pp, respectively. The plus and minus superscripts on the power terms represent a forward (+) and backward (-) propagating beam.

These equations have been used to model the behavior of the amplifier for the case of single or multiple input signals. However, it becomes particularly important to study the amplifier behaviour with mutiple input signals at different wavelengths due to the difference of their absorption and emission cross sections, and thus the different gain coefficients.

2.2.3 Amplified Spontaneous Emission

In the case where the input seed energy is not high enough to extract a significant amount of the stored energy at the seed wavelength, the spontaneous emission can promote a

stimulated emission and become amplified. This process is known as amplified spontaneous emission (ASE).

In the case of a small gain signal in amplifiers and the excessive amplification of spontaneous emission, the fiber amplifier can be overtaken by ASE. In this way ASE must be lumped in with the seed wavelength when calculating the population of the lasers levels, resulting in terms in the differential equation which must be integrated over all wavelengths. The differential equation is given as [14],

$$\begin{aligned}\frac{dN_2(z,t)}{dt} = \frac{D}{hcA}\sum_{j=1}^{J}\lambda_j^p\left[\sigma_a\left(\lambda_j^p\right)N_1 - \sigma_e\left(\lambda_j^p\right)N_2\right]P_p\left(\lambda_j^p\right) \\ + \frac{\Gamma}{hcA}\sum_{k=1}^{K}\lambda_k^s\left[\sigma_a\left(\lambda_k^s\right)N_1 - \sigma_e\left(\lambda_k^s\right)N_2\right]P_s^{\pm}\left(\lambda_k^s\right) \\ + \frac{\Gamma}{hcA}\sum_{k=1}^{K}\lambda_k^s\left[\sigma_a\left(\lambda_k^s\right)N_1 - \sigma_e\left(\lambda_k^s\right)N_2\right]P_s^{\pm}\left(\lambda_k^s\right) \\ + \frac{\Gamma}{hcA}\sum_{l=1}^{L}\lambda_l^{ase}\left[\sigma_a\left(\lambda_l^{ase}\right)N_1 - \sigma_e\left(\lambda_l^{ase}\right)N_2\right] \\ .\left[P_{ase}^{+}\left(\lambda_l^{ase}\right) + P_{ase}^{-}\left(\lambda_l^{ase}\right)\right] - \frac{N_2}{\tau}\end{aligned} \tag{2.74}$$

The equation terms include the population increase in the lasing level due to the pump and the decrease in population of level 2 due to sponatneous emission. Therefore, without special attention to fiber length, the excitation of the gain medium will be depleted by the incoherent ASE rather than by the desired coherent laser radiation. This leads to some optimum length for any laser amplifier.The absorption and stimulated emission are also included for all the wavelengths of the ASE band and seed beam.

2.2.4 Two-wavelength considerations

As a consequence of the electronic structure of Yb^{3+}which gives rise to two different laser actions, a nearly four-level in character at long wavelengths and a truly three-level in character at short wavelengths, it becomes difficult to efficiently amplify multiple input signals in the same fiber that are separated by a substantial difference in wavelength.

Eq.(2.74) revealed that the shape of the fiber gain spectrum is highly dependent on the pump power level. At the low values of pumping, the population will not be fully inverted along the fiber which results in a small signal gain. This leads to the re-absorption of the short wavelengths. Concurrently, longer wavelengths have low absorption cross-section and are less dependent on fiber length.

The emission spectra of Yb in R. Pachotta et. al. fig(1)[39] shows that the ratio of the emission cross section of the shorter wavelengths to longer wavelengths is almost 10 to 1. Due to the dependence of the gain coefficient in Eq.(2.67) on the intensity of the input seed, then it is necessary to optimize the ratio of the input seed energy of the two input wavelengths in order to optimize the ratio of gain of the two amplified colours.

Chapter 3

Experimental Setup and Procedures

The initial study for developing a two-color fiber laser system was done by Dongfeng Liu et. al. in 2004 at the university of Waterloo [13]. The Ti:sapphire laser oscillator was used to generate an ultrabroad bandwidth spectrum out from a 0.5m photonic crystal fiber. For amplification, a two-stage amplifier of double-clad Yb-doped fibers was used to amplify a two-color seed. In the first stage, 135 mW of total average output power was obtained with a significant amount of amplified spontaneous emission (ASE). A notch filter was used after each amplification stage to eliminate the ASE formed near the gain peak of the Yb-doped fiber amplifier. In 2008, Romero-Alvarez et al. [15] developed a dual-wavelength fiber laser system that delivered light at the two wavelengths, 1040nm and 1110nm. The two-color seed of the system was selected from a supercontinuum spectrum which was generated by focusing a 200 mW mode-locked pulses into a 5m photonic crystal fiber (PCF) via Raman conversion. Only 27 mW of the input pulses power remained after transmitting through the PCF, and 5 mW of seed power after selecting the two colors by a notch filter. To amplify the two colors, a two-stage Yb:fiber amplifier was built. For both stages, the Yb:fiber amplifier was of 10m length and of a doping concentration of approximately 1.6% by weight. As a consequence of the low input seed power, a large amount of the output power in the first stage of amplification was ASE. Only 60 mW of the first stage average power (900 mW) was incident into the second amplification stage. The two colors of only 300 mW total average power were then mixed in a nonlinear crystal to generate a mid-infrared radiation.

Due to the fact that the rate of stimulated emission in any light amplifier scales proportional with the pump and signal wave intensities, the present work aimed to increase both the seed energy and the amplification efficiency by having a more efficient supercontinuum

generation and adding a preamplifier which precedes the amplifier chain. To avoid non-linearity with amplification and to accommodate two tunable wavelengths, fiber CPA was employed which has improved the average and peak powers of the whole system. In the CPA system, the pulses were stretched first to support higher powers in the fiber, amplified in a pre-amplifier and a double-clad fiber amplifier system, and finally recompressed by a three grating compressor which generated a shorter and higher intensity pulses. By doing this, difference frequency mixing efficiency should be increased also with these changes added to the previous amplifier system.

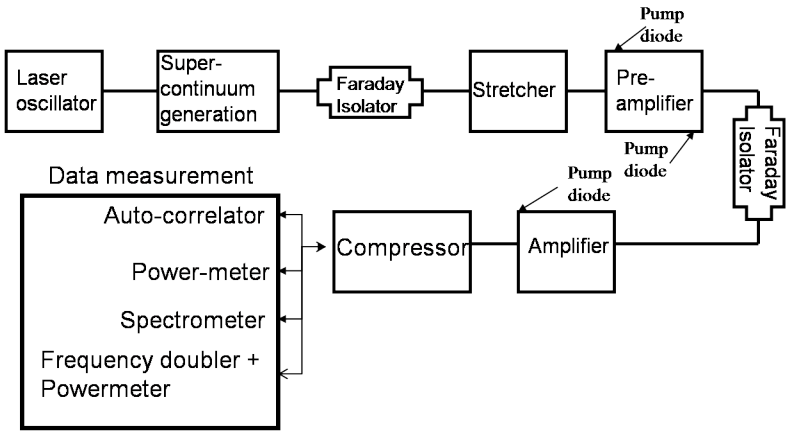

Figure 3.1: Schematic Diagram of the two-color fiber Amplifier.

The schematic diagram of the optical setup of this project is as shown in Fig.(3.1). In brief, a broadbandwidth pulse was generated by focusing the mode-locked pulses into a photonic crystal fiber where the resulting spectrum was then sent to a spectrometer to record the ultra-broad bandwidth. The pulse was stretched to ~30ps by using a bulk grating stretcher. Instead of using a notch filter for selecting the two colors of the system [15], the grating-stretcher system was used. It showed a more efficient way in eliminating seed wavelengths near the gain peak of the fiber amplifier, and thus improve the amplification efficiency at the peak wavelengths of the two color spectrum. As the spectral gain control is not possible in Yb-fiber amplifiers to suppress the ASE at the gain peak, the signal must be stronger than the noise equivalent power of the ASE. Since the two-color seed from the super-continuum generation is still relatively weak, the pulses were first pre-amplified using a double-ended pumping scheme single-clad fiber pre-amplifier, and then further amplified using a double-clad fiber amplifier. After being amplified, the pulses are compressed back

to the femtosecond duration.

By following this general diagram of the experiment, Fig.(3.1), the influence of the double-ended pumping scheme and the use of different pre-amplifier fiber lengths were studied to achieve an optimal gain ratio of the two pre-amplified colors. It was demonstrated that using a pre-amplifier is essential for this system in recompressing the short wavelength pulses back to the femto-second duration. As the gain of a Yb fiber amplifier depends on the wavelength, the power spectrum, and the fiber amplifier length, the optimal length of the fiber amplifier for amplifying the two colors of this system, the 1035nm and 1105nm, was accomplished.

To test the findings, the autocorrelator, the Second Harmonic Generation (SHG), the spectrometer, and a power meter were used to record the data.

3.1 Front-End Laser System

A schematic representation of the setup for supercontinuum generation is shown in Fig.(3.2).

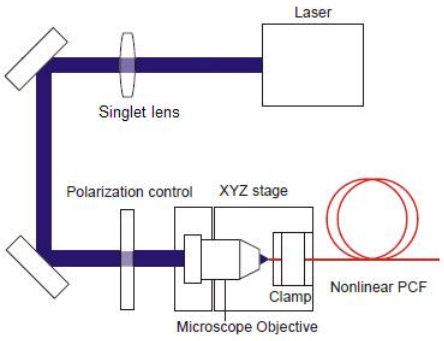

Figure 3.2: Schematic drawing of the setup for supercontinuum generation using the Yb:fiber femtosecond laser and a 2m piece of highly nonlinear photonic crystal fiber [44].

The seed beam of the laser system in this experiment is produced by a 200 mW commercial (Polaronyx) Yb:fiber seed oscillator operating at a peak wavelength of 1030 nm. It generates a pulse train of 200 fs duration at a 50 MHz repetition rate. To collimate the output divergent beam of the laser oscillater, a singlet lens was used of numerical aperture NA= 0.1. The collimated laser beam was then coupled into a 2m PCF length using a 20X objective lens having a numerical aperture 0.4. The PCF used in this work was from the Crystal fiber company (Parts number: SC-5.0-1040) with a zero dispersion wavelength at

1040nm. The fiber ends were carefully cleaned to avoid any possible contamination. Both fiber ends were mounted on a very stable fiber coupler assembly with x, y, z and rotational angle adjustments. This is necessary as the nonlinear effects are inherently very sensitive to variations in the input power. The fiber coupler assembly with PCF was placed after the 20-X objective lens and aligned properly to obtain the best coupling of laser into the PCF. The fiber has an outer diameter of 125 µm, and a solid core of 5 µm in diameter surrounded by a periodic pattern of air-holes, table (3.1). In order to have control on the output spectrum, a half-waveplate was inserted between the laser beam and the input end of PCF .

Material	pure silica
Cladding diameter	125 µm
Coating diameter	244 µm
core diameter	4.8 µm
Zero-dispersion wavelength	1040 nm
NA @ 1060nm	0.2
Attenuation @ 1040nm	<3 dB/km

Table 3.1: Physical and optical properties of SC-5.0-1040 fiber.

Because the nonlinear effects involved in the spectral broadening are highly dependent on the dispersion of the media, the PCF of Institut national d'optique (INO) used by Romero et. al. having the dispersion null at 985 nm [15] was replaced in this work by a one from the Crystal Fiber company (Parts number: SC-5.0-1040) with a zero dispersion wavelength (ZDW) at 1040nm. This type of supercontinuum fiber was used instead since the laser oscillator operates at a wavelength closer to the ZDW of the fiber. This allows the ultrashort high peak intensity laser oscillator pulses to interact with the nonlinear PCF for long distances within the fiber before it temporally broadened by the material dispersion. This will result in a dramatic nonlinear interaction which would generate the widest possible ultra-broad bandwidth spectrum.

At the far end of the PCF, another 20X objective lens was used to collimate the output beam. It was recognised that using this lens provides more transmitted power through the first Faraday isolator of the system than a 10X objective lens would do. This is because of the smaller-size diameter of the collimated beam that the former lens provides. As it collimates the beam into a smaller diameter size, less fraction of the incident beam is diffracted by the edges of the isolator.

Due to the small core size of the supercontinuum PCF, table (3.1), a critical alignment was required to have a stable input power going through the fiber. This was difficult to maintain over an extended period of time due to the surrounding effects. To help minimize these effects, the fiber was placed in a plastic box.

The spectrum from the PCF output was investigated with an optical spectrum analyzer (Ando AQ-6310B) which has a full spectrum range from 400 nm to 1750 nm with a resolution of 0.2nm.

From the fiber coupler, the beam passes through another half-wave retarder plate and then through a Faraday isolator. The Faraday isolator allows only polarization of 45 degrees to enter, and then rotates the polarization of the output by 45 degrees so it exit in the vertical direction. This is accomplished by using a pair of polarizers in conjunction with a Faraday rotator, an element that applies a magnetically induced direction-dependent rotation to the polarization of the beam via the Faraday effect. In this way a beam passing though the isolator and bouncing back will be rotated through a total angle of 90 degrees. This ensures that backwards traveling beams do not propagate beyond the isolator and damage the sensitive seed laser system. The half-wave plate is inserted to maximize the signal passing through the initial polarizer.

Since the PCF used in this experiment is a high birefringent fiber, the seed beam coming out from the fiber is elliptically polarized. Therefore, the seed beam is split by the first polarizer of the Faraday Isolator, and the rejected polarized beam is blocked by a black shield to prevent stray laser light in the lab.

3.2 Grating Stretcher

To stretch the 200fs ultrabroad bandwidth pulses, the seed beam was sent after the first isolator into the grating stretcher system. Using this system, the spectrum was spectrally separated and isolated from the unwanted frequencies. However, due to the small size of the transmission gratings used for this system, only 20 mm x 10 mm, stretching a seventy nanometers apart colors was not possible in a single grating line. Accordingly, a three-grating system was used. The stretcher system layout is depicted in Fig.(3.3).

The three gratings were placed anti-parallel with a telescope between them. The transmission gratings used were from Ibsen Photonics with a 1250 lines/mm. The lenses used for the telescope were an anti-reflecting coating lenses. These lenses provided less power loss. They are of 300 mm focal length. In order to have the beam collimated after passing

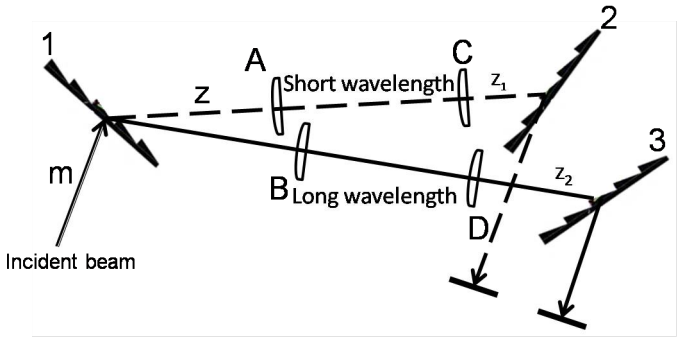

Figure 3.3: The stretcher setup. The diffracted spectrum is splited into two colors which each is stretched seperately.

through the telescope, the two lenses were placed at 61.5 cm separation distance. The first grating of the stretcher, shown in the left side of Fig. (3.3) was placed a 6 inch, or a $\backsim$15 cm, away from lenses A & B. At a closer separation distance, the two colors would not have enough free space to spatially separate and pass through the two lenses, A and B. Lense B was placed a bit farther, just behind lense A, from grating 1 as this separation distance (6 inchs) was not even enough for the two colors to be widely separated. The two lenses were adjusted so the two colors were contained and propagated through the center of the two lenses. The range of frequencies between the two colors stroke first, before being isolated from the two colors by slits, the edges of the lenses A and B. To change the amount of stretching, gratings 2 & 3 were moved forward and backward from lenses C and D. z_1 and z_2 were set not equal. In the compressor, at these amount of stretching, the angle of the spatial separation of the two colors is small for the two gratings to be placed at the same separation distance and while containing the compressed pulses. By setting the separation distance not equal, the two gratings were placed behined each other so that they contain the two colors.

To measure the amount of pulse stretching, the equation from Treacy [20] was used:

$$stretched\,pulse\,duration = 2 \times \frac{b\,(\lambda/d)\,\delta\lambda}{cd\left[1-(\lambda/d-sin\theta_i)^2\right]} \tag{3.1}$$

The equation is multiplied by a factor of 2 as stretching is done by a double pass through the stretcher system.

As it was seen in the previous chapter, inserting a stretcher in front of the amplifier

chain system is to avoid fiber nonlinearity by reducing the seed pulses peak power. In order to stretch the laser oscillator pulses, the input beam had to undergo a double-pass in the same vertical plane through each of the three gratings. It was difficult to keep the beam contained by the grating with an input beam collimated by a 10-X objective lense. This would lead to a partial loss of the seed power before being sent to the pre-amplifier. For this, another advantage of using the 20-X objective, rather than the elimination of the diffraction by the edges of the first isolator, is to collimate the output beam of the PCF with a radial size that is appropriate for building the stretcher system.

In this experiment, the stretcher was mainly used as a wavelength selector as the power of the system was relatively low for nonlinearity. The use of the transmission gratings provided a high diffraction efficiency of 97% in the first order of diffraction. The collimated light from the laser was s-polarized by the polarizer of the faraday isolator and incident upon the grating to provide a maximum diffraction efficiency. As light passes twice through each of the three gratings and through the telescope air lenses, the loss created by the optical components was around 22 % from total input power.

To build this stretcher and to generate a spectral chirp in the incident pulses, the beam was aligned so that it propagated in its first pass through the whole system in the same horizontal plane through path m even after the insertion of the telescope. This was done by using two mirrors and two irises. By using a two mirrors, the beam was directed to enter at the bottom part of the first grating. For maximum diffraction efficiency, a power-meter was placed after the grating to measure the minimum transmission power, and thus maximum diffraction power, while rotating the first grating around its vertical axis. After being diffracted the beam must travel in the same horizontal plane, unless there is an orientational misalignment when mounting the grating. This misalignment will lead also to a residual spatial chirp at the output of the stretcher. A proper mounting can be done by placing the used irises at a far diffracted distance from the grating and fix any oriental misalignments. For this, lenses were inserted in the diffracted beam path while making sure, by using the irises, it maintained its height. By doing so, the beam passed exactly through the bottom part of the other two gratings; mounted using the same grating mounts. The back mirrors were aimed slightly upwards so that the beam was directed to the top of lenses A & B in the telescope to refract then downwords through the top part of the first grating to a lowered mirror where the pulses were recombined and sent into the pre-amplifier fiber, Fig.(3.4).

The selection of the desired bandwidth of the two colors were controlled by inserting

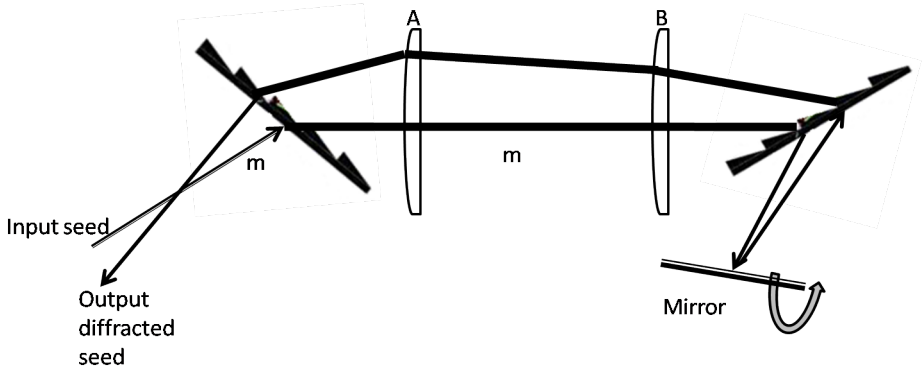

Figure 3.4: The stretcher setup. The diffracted spectrum is splited into two colors which each is stretched seperately.

slits at the focal point of the telescope lenses. Isolating the bandwidth is neccesary in fiber amplification as a seed with a broader bandwidth than required may spread the gained energy into unwanted wavelengths, and thus lower the energy for the required seventy nanometer apart colors.

3.3 Double-ended Fiber Pre-amplifier

In this thesis, a further improvement of the output average power of the two color fiber amplifier system achieved by Romero et. al [20] was reported. To accomplish this, the energy of the two colors incident into the first stage amplifier had to be increased. Since the seed signal from the super-continuum was still not strong enough to compete with the ASE of a high power fibre amplifier, a pre-amplifier stage was added to the amplifier system.

For the pre-amplifier, a single-slad single-mode Yb 1200 4/125 fiber was used with two 975-nm diode-stack sources pumping at an identical maximum average power of 150 mW in a double-ended pumping scheme. However, to pump conventional single-clad fibers, where just the rare-earth-doped single-mode core can guide light, spatially coherent pump sources are required. These fibers can be highly doped so the lengths can be short, thereby reducing nonlinear effects. They are also compatible with low-cost low-power pump diodes. Single-clad single-mode fiber makes an excellent preamplifier in a fiber amplifier chain with double clad fiber acting as a power amplifier. The characteristics of the fiber used is mentioned in table (3.2).

Material	pure silica
Cladding diameter	125 µm
Cladding Geometry	Round
Coating diameter	245 µm
core diameter	4.8 µm
Cutoff wavelength	1010 nm
core NA	0.2
Attenuation @ 920 nm	280 dB/m

Table 3.2: Physical and optical properties of Yb 1200 4/125 fiber.*http://www.thorlabs.com*

The experimental setup of the pre-amplifier is shown in Fig.(3.5). The pump beams were launched through opposite ends of the active fiber via collimating and focusing lenses and a pair of standard mirrors. The fiber ends were polished at an angle of 8° to prevent parasitic lasing. The low energy two-color seed was directed and focused into the fiber by a short wave pass (SWP) dichroic mirror with high reflectivity in the seed wavelength range and a 10-X objective lens, respectively. At the output of the system, the signal was separated from the pump beam using another SWP dichroic mirror having high transmission at the pump wavelength and high reflection at the seed wavelengths. The amplified seed beam passes through a half-wave retarder plate and then through a Faraday isolator.

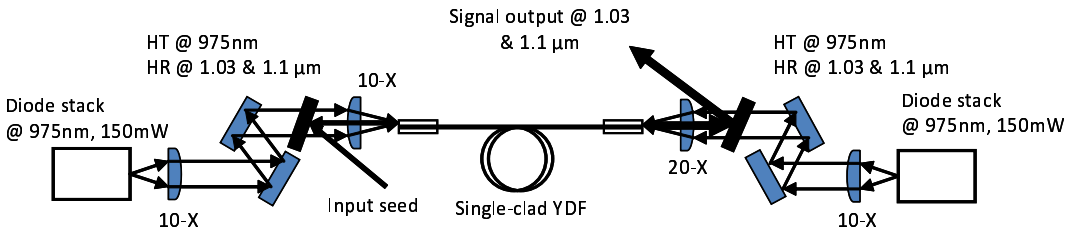

Figure 3.5: YDFL experimental arrangement with two diode-stack pump sources. HR: high reflectivity, HT: high transmission.

Ytterbium is relatively transparent to 1105nm, having a much lower absorption cross section at this wavelength than at 1035 nm [39]. The alignment of the long wavelength through the core can easily be accomplished even if the pump is not running, whereas the 1035nm light in the core can hardly reach the end of the fiber for detection. To record the spectra of the two colors at the output of the pre-amplifier system, the ANDO spectrometer was used. The beam had to be focused first into a standard single mode fiber which was

connected to the spectrometer. This fiber was also used in this stage to help align the two colors through the fiber pre-amplifier. As the two-color beams propagate through two different paths in the stretcher, Fig.(3.3), aligning them into a small size core, highly doped Yb fiber is not easy especially with the high absorption of the 1035nm. As a first step of alignment, the two-color beams were focused into the standard single mode fiber by using the back mirrors of the stretcher. This leads the two beams to propagate nearly in the same plane of propagation and makes the alignment of the two-color beams through the pre-amplifier much easier.

To align the pump and the seed beams, a power meter was placed at the opposite end of the input side to the pre-amplifier fiber. To obtain maximum coupling efficiency, it is essential that the laser beam travels along the optical axis of the microscope objective. Using two mirrors, the laser and the pump beam were aligned with the optical axis. For the two colors alignment, the long wavelength was firstly coupled. When the experiment was ready to operate after the alignment of the long wavelength color and the pump, the 1035nm beam was then optimally aligned using the back mirror of the stretcher. This was done by detecting either the output average power of the amplifier system or via the spectrometer. A fiber coupler was used to mount the microscope objectives and the fiber. At the input seed side, a 10-X objective was used rather than a 20-X since the beam coming from the stretcher was relatively large that it was striking the edges of the 20-X objective. At the opposite side, a 20-X objective was again used to collimate the divergent output of the pre-amplifier fiber. As explained previously, this eliminated the diffraction of the collimated beam by the edges of the isolator. A notch filter was placed after the preamplifier to eliminate the ASE formed at this stage. A Faraday isolator was placed before the second amplification stage to eliminate backwards amplification.

It has been discussed in chapter 2 that YDF laser systems exhibit a strongly wavelength-dependent gain profile due to the spectroscopic properties of the Yb^{3+}dopant. For wavelengths below 1075nm, the Yb:fibre amplifier has a quasi three level behavior. Without pump power there is a strong absorption and the seed would not survive to the other fiber end. Above 1075nm, it has nearly pure four-level behavior. The gain is proportional to the overall upper-state population (e & f Yb sublevels) and the re-absorption is very weak. Because of this dual laser behaviour, and the dependence of the gain of the Yb fiber amplifier on the length of the Yb fiber, a study of the optimal fiber length for amplifying the two colors was essential in this project to obtain the optimal gain ratio of the two colors for this laser system. As the gain is a function of the pumping power, a study also was made for

the importance of the double-ended pumping scheme on the output gain at the two colors of the system.

3.4 Double-Clad Fiber Amplifier

After the isolator, the beam enters the fiber amplifier of the system. This stage comprises a double-clad fiber, a 7 W pump diode operate at 975 nm, two fiber couplers, a two microscope objectives, standard and gold mirrors, and a SWP filter. At the input of the fiber end, a 20-X microscope objective lens focuses the incident light onto the fiber. To align the pre-amplified seed into the fiber amplifier, two mirrors placed infornt of the fiber coupler or one mirror and a fiber coupler with x, y, z adjustments were required. The optimal coupling can be achieved by measuring the output power at the other end of the fiber amplifier by the powermeter. When the amplified seed beam emerges from the fiber amplifier, it passes through a 10-X microscope objective lens which at the same time collimates it and focuses the 975nm pump light from the 7W diode source into the fiber. The output of the amplification stage will then be reflected off by a dichroic mirror coated to allow transmission at 975nm pump beam while reflecting the two colors into next stages.

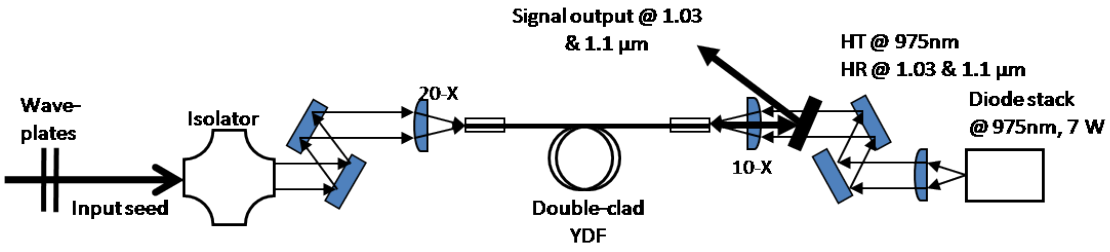

Figure 3.6: The schematic diagram of the amplifier.

The 7W pump source is coupled and affixed to a fiber coupler. The pump is collimated with 10-X microscope objective lens to allow good coupling into the inner cladding of the doped fiber3.6. After the dichroic mirror the amplified two color seed travels through another half-wave plate, and then sent into the compressor.

The fiber amplifier at 1035nm and 1105nm consists of an all silica, double-clad, ytterbium doped fiber pumped at 975nm. An optical fiber, generally referred to as step-index fiber, consists of a central glass core surrounded by a cladding layer of different refractive index. Many modes of the laser can propagate down the fiber unless the waveguide is made

with a small enough diameter where only one mode can be totally internally reflected down the fiber. These fibers are called single-mode fibers and are available with single-clad and double-clad layer.

The efficiency of coupling the pump power into a doped core where it overlaps with the signal determines the amplification in optical fibers. Generally, high-power pump diodes of several watts have multimode beams where for this double-clad fiber is typically used. Here, the active doped core is surrounded by a second waveguide, which is highly multimode, and on the order of hundreds of microns, Fig.(3.7). In this second waveguide, also called inner cladding or pump core, low brightness high power diode lasers can be easily launched. This pump light is gradually absorbed over the entire fiber length and is converted into high brightness high power laser radiation. Laser light, guided in the core through the principle of total internal reflection, is generally introduced at one end of the fiber.

Different seeding geometries (shining seed colors from different sides) using a double-clad fiber were studied by many groups in the case of two color input seed. The study showed minor effects on the amplified signal gain and the amplifier performance. Nevertheless, launching the seed in the backward direction is the most preferable as it is easier to configure than any other seeding configurations.

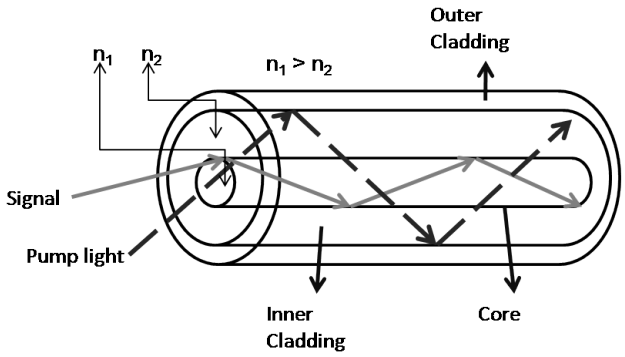

Figure 3.7: Schematic diagram of the double-clad fiber. The signal light is coupled into the fiber core where it is amplified by the pump light, which is coupled into the inner-cladding and absorbed by the doped core of fiber.

In addition to what previously mentioned, amplification is achieved when fiber contains dopants that laser light can excite, thus causes stimulated emission in the manner described in chapter two. Besides, a special attention must be considered of the fiber lengths when amplifying short wavelengths and systems of dual wavelength seed.

For the two signal wavelengths used in our experiment (1035nm and 1105nm) that are close to the two color wavelength used in Budz et. al. experiment, i.e. 1040nm and 1100nm, the results indicated that the optimal fiber length for amplifying 1040nm is around 4m while the amplification of the 1100nm shows less sensitivity to the fiber length.

According to his paper, the optimal length, measured by simulations, for the two amplified signals to experience the same net gain was found to be 6.8m. The work revealed that the shape of the fiber gain spectrum is highly dependent on the pump power where at low values of pumping, the upper-state population density at the seed end of the fiber becomes low enough for stimulated emission and thus leads to the re-absorption of the 1040nm. Therefore, the gain bandwidth of fibers depends on the power and wavelength of the pump beam, the concentration of the doping ions and the energy of the input seed.

For generality, the above description were considered for a double-clad fiber. However, the analysis applies to single-clad fibers as well. The only difference of the simulation is that the confinement factor of the pump is less than that of the seed for double-clad fibers, but for single-clad fibers they are the same.

However, to ensure the propagation of the pre-amplified seed is through the single mode core of the fiber and not through the inner cladding, an optical diode with an oscilloscope was used to measure the gain of the pre-amplified seed. To accomplish this, the pump was first coupled with a powermeter placed at the opposite end of the input pumping fiber end. It was used to measure the maximum output forward average power that can exit from the fiber at the maximum coupling efficiency. However, this does not necessarily tells that the pump is significantly absorbed through the core of the fiber and is being emitted as an ASE. For this reason, the ASE backward output power of the fiber amplifier was then measured. This corresponds to the optimal coupling, the one that ensures the maximum absorption of the pump through the core of the fiber. The long wavelength was then coupled with a powermeter placed at the opposite end of the fiber to measure the maximum average power passing through the different fiber layers. To have the pre-amplified long wavelength propagate through the doped core and be amplified, an optical diode connected to an oscilloscope was placed at the input pumping side of the double-clad fiber. At the beginning the pump driver was set at 2A without any signal incident into the fiber. When the optical diode was adjusted by centering it through the backward ASE beam, a DC voltage level was observed by the oscilloscope. The coupling of the pump was optimized by having the highest voltage level. The pre-amplified seed was then let to go through the fiber, and photon amplitude pulses were observed on the oscilloscope

corresponding to the amount of gain at the long wavelength in the fiber. The coupling of the pre-amplified seed was optimized through the core by moving the knobs of the two gold mirrors placed before the double-clad fiber while observing the amplitude of pulses presented on the oscilloscope.

3.5 Three-Grating Compressor System

A three-grating compression system was used to compress the two-color output from the amplifier, which is based on a standard negative dispersion grating compressor [20]. Identical transmission gratings were used in both the stretcher and compressor. As mentioned in chapter 2, light traveling in transparent material will come under the effect of material dispersion. When light of long wavelengths travels faster than light of short wavelengths, the light is said to have a linear positive chirp. This is observed in normal transparent media where light is positively dispersed.

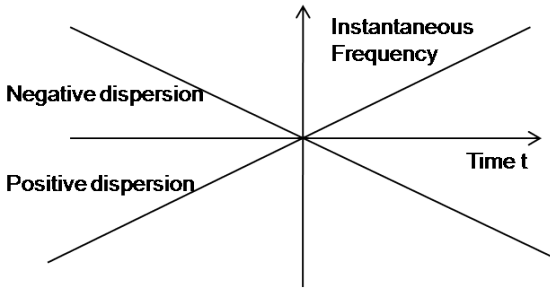

Figure 3.8: Positive and negative frequency chirp as a function of time.

After pulse being stretched through material dispersion, another system is needed to recompress the stretched pulses by applying a negative chirp and compensate all the dispersion orders.

The collimated light from the amplifier was *s*-polarized by a wave-plate and incident upon the grating to provide a maximum diffraction efficiency. The other two gratings were aligned parallel to the first grating.

The incident beam was aligned so that it propagates through the top part of the first grating in the same horizontal plane. This was again done by using two mirrors and two irises, and a powermeter was used also to adjust the first grating for maximum diffraction efficiency. This way, the incident angle into the stretcher and the compressor will be the

same, and the effect of the third order dispersion due to the mismatch between the gratings of the stretcher-compressor system will be canceled. As the two colors diffracted separately by the last two gratings, the beam was redirected towards the rest of the experiment by using plane mirrors which were tilted slightly downwards towards a lowered mirror earlier in the setup, Fig.(3.9).

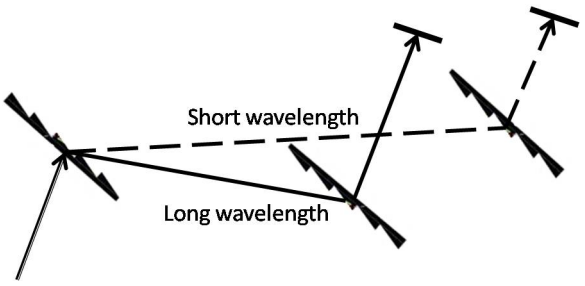

Figure 3.9: The compressor setup. The two colors are recompressed separately.

To demonstrate the cancelation of the spatial chirp after the compressor, i.e. misalignment of the compressor gratings, the seed was detected by a spectrometer. When there is a large angular errors between the gratings of the compressor, residual angular dispersion causes the rays to not be parallel. In this case, the wavelengths will not recollimate after the double pass through gratings, and spatially smearing occurs. The total energy will not be contained within a circle. When focusing the output beam into the blue fiber of the spectrometer and the coupling is changed by the back mirror of the compressor, the smearing that occured in the output beam can be detected by the spectrometer as a function of the angle of rotation of the back mirror.

As the two amplified colors passes through each of the three gratings in the compressor twice, a loss of 12 % is expected if the incident beam was linearly polarized. However, because the fibers used in this system were not polarization maintining (PM), the polarization after the single mode fibers was elliptically polarized which causes more loss by this system. There was no real accurate measurements of the loss by this system at the two colors as the spectrum incident to the compressor system had a significant amount of ASE.

3.6 Autocorrelator

The most useful tool for estimating the duration of femtosecond optical pulses is an autocorrelator. Pulses of duration less than 1ps cannot be detected by an oscilloscope or photodiodes, this is because the response time of optoelectronics is at the best around 200fs. For this, the autocorrelation signal is generated by second harmonic generation (SHG). The generation of the second harmonic in crystals is a nonlinear process that requires high peak intensity. However, such high peak intensity can be obtained by shortening the pulse duration of ultrashort pulses using the compressor, and as a result the intensity autocorrelation function, $A_{SHG}(\tau)$, is often measured experimentally.

To measure the autocorrelation signal, the compressed beam was splited 50:50 by a splitter. The two beams passed then through a 50 % splitter and raised up using a right-angle mirrors where they were sent again through the splitter. The two parallel beams with a variable delay were generated and then focused using a singlet lens. They were recombined in a $\chi^{(2)}$ crystal (BBO) and the power of the second-harmonic signal at each delay point was measured with a time-integrating linear photomultiplier.

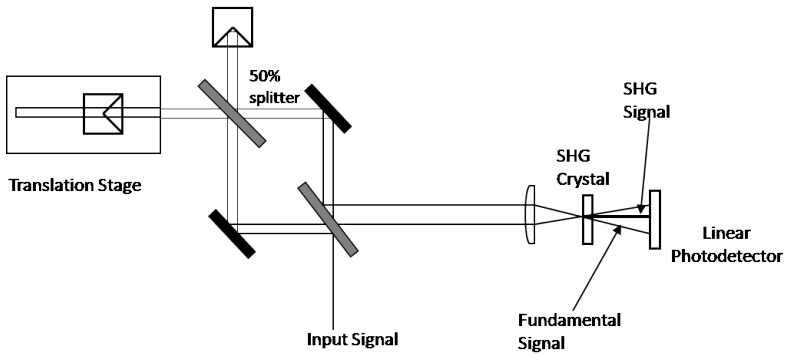

Figure 3.10: SHG-based Autocorrelation using a Michelson interferometer and a $\chi^{(2)}$ crystal.

After passing through the crystal each color will undergo a SHG, while the autocorrelation SHG signal will be spatially separated from the fundamental beams, allowing the autocorrelation to be background free. At a given delay point, τ , the autocorrelation signal generated in the nonlinear crystal is described by

$$E_{SHG}(t,\tau)\,\alpha\,E(t)E(t-\tau),$$

where $E(t)$ is the electric field of the compressed signal beam under test and $E_{SHG}(t,\tau)$ is cross signal at the second-harmonic frequency, and the intensity of the second-harmonic signal can be described by

$$I_{SHG}(t,\tau)\,\alpha\, I(t)I(t-\tau).$$

Sampling the second-harmonic signal as a function of the delay, τ , with the time averaged linear detector produces the characteristic autocorrelation function, $A_{SHG}(\tau)$, of the signal

$$A_{SHG}(\tau) = \int_{-\infty}^{\infty} I(t)I(t-\tau)dt.$$

This is a direct multiplication of the electric fields using a $\chi^{(2)}$ process, which is subsequently converted to intensity in the linear photodetector.

To calculate the correlation width of the SHG pulse, the following equation was used:

$$Correlation\ duration = \frac{(line\,delay)_{FWHM}}{c} \times 2$$

However, for a gaussian pulse the autocorrelation width is $\sqrt{2}$ longer than the signal width. Therefore, readings the has been done in this thesis were divided by $\sqrt{2}$ in order to calculate the pulse width instead of the correlation width.

3.7 Second-Harmonic Generation

A doubled frequency or second harmonic generation takes advantage of second order non-linear terms in the polarization of various materials [34],

$$\mathbf{P} = \epsilon_{\mathbf{o}}\mathbf{E}[\chi^{(\mathbf{1})} + \chi^{(\mathbf{2})}\mathbf{E} + \chi^{(\mathbf{3})}\mathbf{E^2}\ldots] \tag{3.2}$$

where E is the electric field, χ is the susceptibility and ϵ_o is the permittivity of free space. The second order non-linear susceptibility, which depends on the symmetry of the crystal medium used for doubling, takes the form of a nonlinear coefficient, d_{eff}, with the appropriate symmetries and transformations[34].

The simplest case for analysis of second harmonic generation is a plane wave of amplitude

$E(\omega)$ traveling in a nonlinear medium in the direction of its k vector. A polarization is generated at the second harmonic frequency

$$P(2\omega) = 2\epsilon_o d_{eff}(2\omega, \omega, \omega)\, E^2$$

In terms of the optical intensity, $I = n/2\sqrt{\epsilon_o/\mu_o}\,|E|^2$, it can be concluded that the intensity of the SHG, $I(2\omega)$, is proportional to the square of the intensity of the input signal, $I^2(\omega)$.

A measurement of the second harmonic generated signal helps determine the pulse intensity. If the 10nm bandwidth comes from ASE rather than amplified signal the temporal duration will be DC and therefore have low intensity and give small green signal. On the other hand if it is amplified signal, the pulse will be short $<$100ps and generate significantly more green. For this reason, the frequency doubled power gives a measure of pulse of ASE power ratio.

The SHG of the two colors was accomplished using a Barium Borate crystal (BBO). Because of the polarization dependence of the BBO, the amplifier output beam should pass first through a half-wave retarder plate, then through a lens to ensure sufficient phase matching within the crystal, and finally through the BBO leaving an output which contains both input signal wavelength radiation as well as doubled radiation. Before measuring the power of doubled radiation, the signal light is eliminated using a blue optical filter, allowing the green color (500 nm range) to proceed into the power meter diode.

Chapter 4

Data description and Results

After the achievement of Romero et. al [15] in building a two-color fiber amplifier system for mid-infrared radiation, the primary aim of this study was to build a more powerful two-colour ultrashort laser system. This is to have a more efficient production of mid-infrared radiation. To maximize the output power of the system, we had to rebuild and fine-tuned each part of the system. This was established by utilizing Chirped Pulse Amplification (CPA) and adding a pre-amplifier into the amplifier chain.

To demonstrate the usefulness of adding a pre-amplifier into the amplifier chain of this fiber laser system, several studies were made on the behaviour of the pre-amplifier with the different input seed energies, bandwidths isolation, and fiber lengths. As in any experimental investigation, this study experienced a period of trial and error when developing and fine-tuning the pre-amplifier. As such, out of a thousands of trial hours, attention turned to the isolation of the unwanted input seed fequencies into the pre-amplifier and to the alignment of the long wavelength seed to the pre-amplifier fiber before the short wavelength. The last seed wavelength was coupled with the fiber as best as possible. Many of the issues encountered were to do with the stability of the supercontinuum spectrum and the recompression of the short wavelength.

4.1 Supercontinuum

At the beginning of the study, the 50nm notch filter, an interference filter, was placed to select the two input color seeds which were generated from the photonic crystal fiber [Institut national d'optique (INO)] having the dispersion null at 985 nm. The seed energy

at the 1105nm was not signficantly high. The average power after inserting the notch filter was only $P_{seed} = 1.11mW$. Fig.(4.1) shows the result after amplifying the two-color seed by the pre-amplifier. To obtain this graph, the pre-amplifier was pumped from each side with 65 mW. Thus the total pumping power was 130 mW. The output average power measured of the amplified seed was 9mW. The figure shows a significant amount of ASE in the wavelength range 1050 to 1080nm. As there was not much energy at the long wavelength, and as this moderate seed power was not high enough to extract a signficant amount of energy stored by the pre-amplifier at the seed wavelengths, the INO PCF was replaced by the SC-5.0-1040 PCF. This was to generate a spectrum that gives a significant amount of energy at 1105 nm, and thus enhance the amplification of this wavelength.

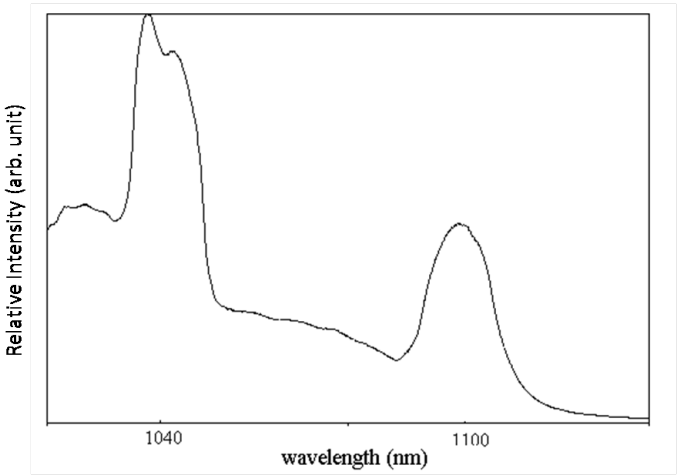

Figure 4.1: Two-color spectrum generated from INO PCF after being amplified in a single stage by a 2m pre-amplifier.

The dispersion of the photonic crystal fiber can be tuned by scaling the sizes of the fiber structure and the distribution of the air holes. The single-mode, nonlinear photonic crystal fiber SC-5.0-1040, has a zero dispersion around 1040 nm. As the pump wavelength of 1030 nm was close to the PCF zero dispersion wavelength, the measured spectrum broadening was relatively flat with spectral range from 900 nm to 1175 nm. The nonlinear interaction of the laser femtosecond pulses with the nonlinear PCF leads to this spectral broadening. An example of the spectrum from the PCF output was investigated with an optical spectrum analyzer (Ando AQ-6310B) which has a full spectrum range from 400 nm to 1750 nm with a resolution of 0.2nm, Fig.(4.2).

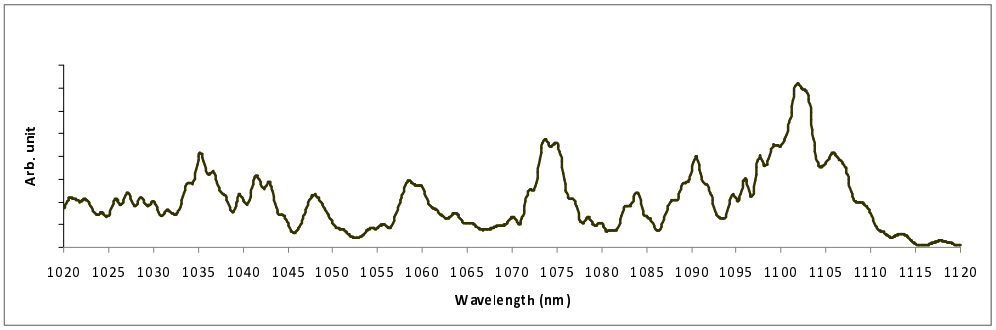

Figure 4.2: Supercontinuum generated in a nonlinear fiber with zero dispersion at 1040 nm by pumping with femtosecond pulses at 1030 nm.

From the figure, it is abvious that the spectrum has peaks at the two colors of the system, the 1035 and 1105nm. However, this spectrum was not obtained at the maximum output power from the PCF. The two mirrors before the fiber, Fig.(3.2), were tweaked to have this spectrum.

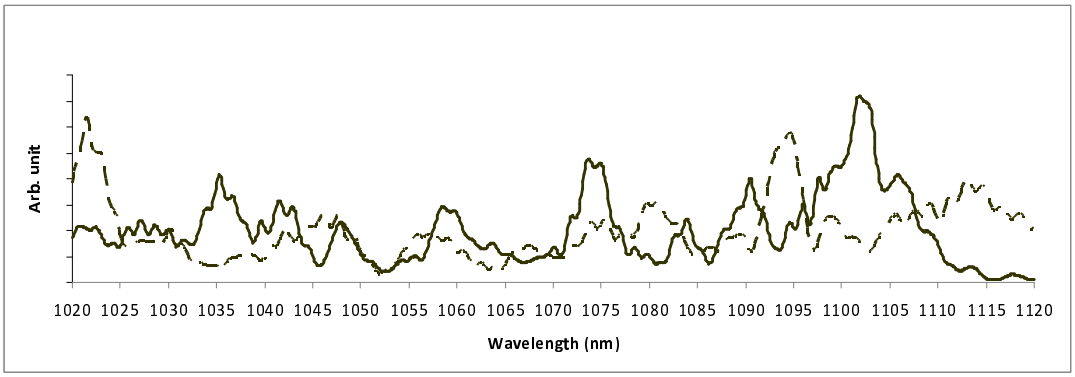

Figure 4.3: The change of the supercontinuum spectrum due to the changes in the coupling with the PCF.

As the supercontinuum generation is so sensitive to the coupling efficiency, hundreds of spectra were obtained out from this PCF during this study. There was no certain position that we can refer to obtain the same spectrum each time. To have the suitable spectra, the output beam from the fiber was monitored by the spectrometer while tweaking the mirrors until a suitable spectrum was obtained with peaks at the two required colors regardless of the average output power. However, it was not always possible to have a suitable spectrum with

a significant energy at the two colors. Due to surrounding effects, such as the movements of the lab table during the work, the coupling with the fiber was contineously changing, and thus the output spectrum changed also. This had a large impact on the progress of the project. An example of this change is shown in Fig.(4.3).

The two spectra in the figure show a difference in the energy at the two colors, the 1035 and the 1105nm. As previously mentioned, the gain is not saturated in the amplifiers and so the output power depends on the incident energy of the signal. For this reason, it was not easy through out the whole study to achieve the goal set for this project.

4.2 The Pre-amplifier study

As a first trial to select the two colors of the system, we chose the notch filter to isolate the unwanted frequencies. The notch filter was placed after the first isolator, Fig.(4.4). The average output power from the PCF was 34 mW. After the first isolator only 15 mW remained due to the block of the signal polarization components by the initial isolator polarizer. Only 8.5 mW remained after the selection of the two colors by the notch filter.

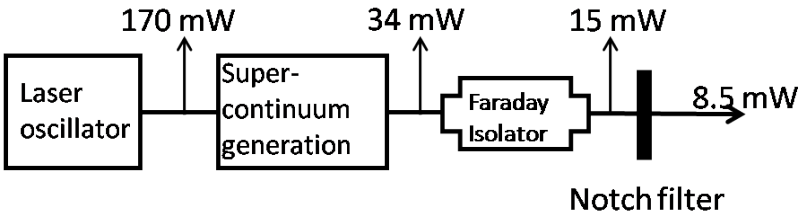

Figure 4.4: Schematic diagram for the notch filter.

However, using the notch filter only blocks a 50nm spectral bandwidth allowing a significant amount of nergy to be incident into the pre-amplifier at unwanted frequencies. Fig.(4.5) shows an example of a spectrum after a notch filter.

The two-color seed was focused into the pre-amplifier fiber. Fig.(4.6), is the output spectrum after the pre-amplifier. The readings were recorded while pumping at maximum power ($P_p = 150\,mW$) from each side of a 2m fiber pre-amplifier. The output average power measured by the powermeter was 23 mW. As the wavelengths above 1040nm and below 1100nm were not blocked by the notch filter, a significant amount of energy was gained at wavelengths below 1100nm and at 1040nm. These wavelengths are closer to the

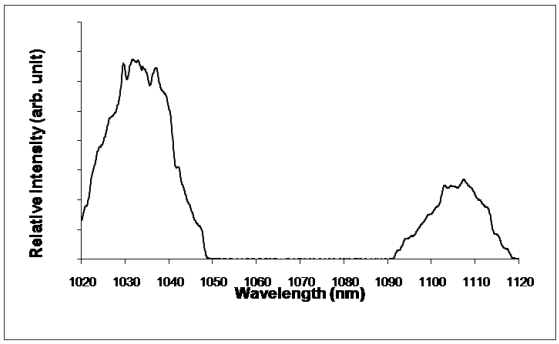

Figure 4.5: Seed spectrum after a notch filter.

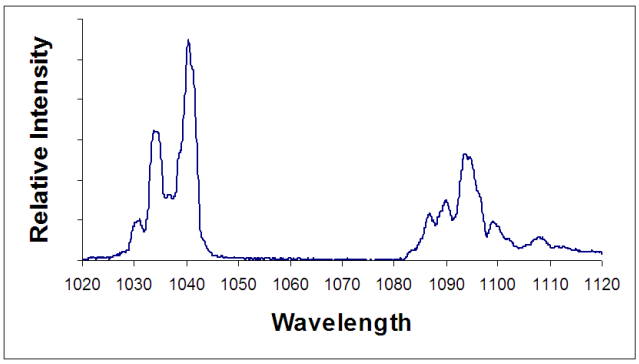

Figure 4.6: The amplified seed of fig.(4.5) after the pre-amplifier.

fiber amplifier gain peak and are preferentially gained. This had lowered the gain at the desired colors, the 1035 and 1105nm.

The isolation of the frequencies can be controlled by rotating the notch filter. In a trial to stop the gain at 1090 nm, the notch filter was rotated such that it allowed more of the short wavelengths to be incident to the pre-amplifier. However, this has prevented the emission at the long wavelengths below 1090nm but concurrently, allowed the emission of an enormous amount of energy at wavelengths above the 1040nm, Fig.(4.7). This had lowered the gain at the long wavelengths as the gain peak of Yb doped fibers is at 1050nm. The output average power was 30 mW.

The two amplified spectra shown in Figs.(4.6&4.7) were not useful for this system, as the goal was to increase the energy at wavelengths of seventy nanometers apart.

After many trials trying to optimize the gain of the two colors using the notch filter for

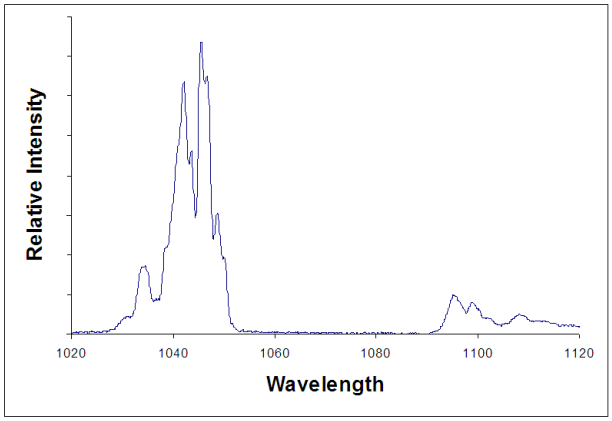

Figure 4.7: The amplified seed after the rotation of the notch filter to block long wavelengths below 1100nm.

isolation, we turned the attention to use the stretcher as a wavelength selector. The slits were placed at the focal length of the telescope lens, midway between the two lenses. This gives us flexibility in selecting the bandwidth of the seed, coupled into the pre-amplifier. The spectrum shown in Fig.(4.8) is an example of the seed after the stretcher.

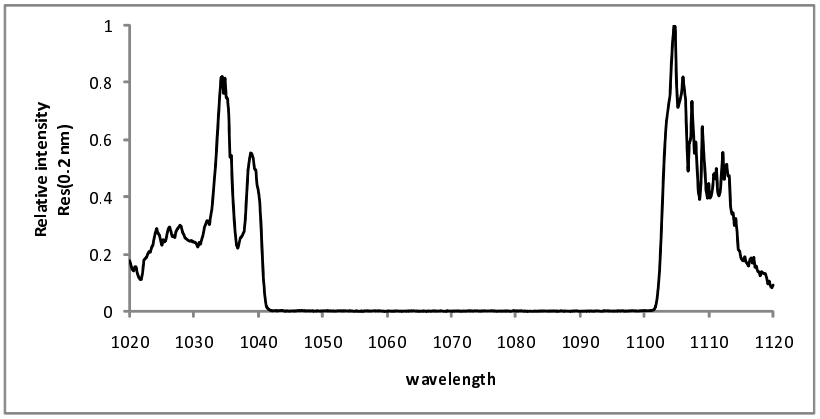

Figure 4.8: The seed after the stretcher with average power of 4mW. The resolution of ANDO is 2nm.

To have this spectrum after the stretcher, we had first to tweak the mirrors before the PCF to have the peaks at the two colors as shown in Fig.(4.2). To select the two colors, the spectrum after the stretcher was monitored by the spectrometer. The wave-plate, before the first isolator, was rotated to maximize the energy at the two colors and then the two

colors were isolated, by using slits, from the unwanted frequencies. The average power after the first isolator was 18mW and 4.6 mW after the stretcher. However, wavelengths below the 1030nm were not blocked. These wavelengths are not strongly amplified by Yb amplifiers due to the gain competition with wavelengths above 1030nm.

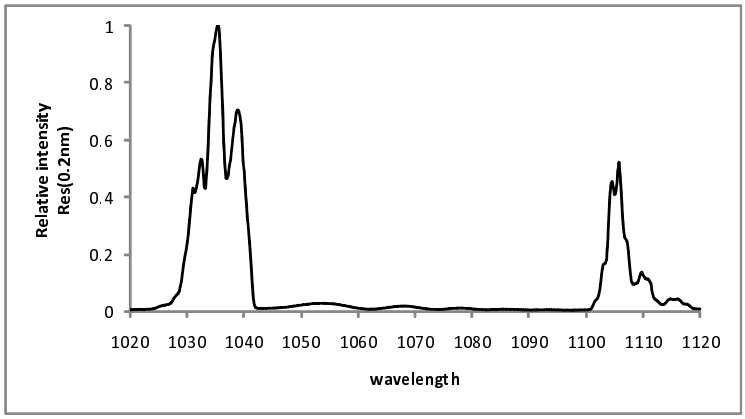

Figure 4.9: The spectrum of a 2m preamplifier at maximum pumping power (150 mW).

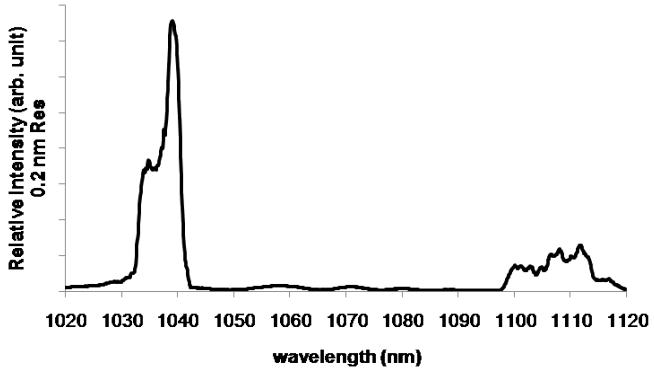

Figure 4.10: Another example of amplified seed by pre-amplifier due to the change of the supercontinuum spectrum.

To amplify the pulses by the pre-amplifier, a 2m fiber length was used at the begining. Pumping from each side with 150 mW, the average output power was 20 mW. Fig.(4.9) shows the output spectrum after the pre-amplifier. To obtain this spectrum the long wavelength was first coupled with the pre-amplifier fiber. The short wavelength was then coupled as best as possible. This was done while measuring the average output power after the pre-

amplifier. From Fig.(4.9), it can be seen that the gain is only at the wavelengths below the 1040 and above 1100 nm. Although, there is still some ASE present at the output spectrum. The seed is still not high enough to extract all the stored energy in the fiber.

However, as the spectrum from the supercontinuum fiber was not stable, Fig.(4.3), many spectra with different gain ratio of the two colors were obtained from the same fiber length and the same device configuration. Fig.(4.10), is another example that was obtained from the pre-amplifier. The output power of 28 mW was higher than that obtained in Fig.(4.9). According to the amount of energy that was obtained from PCF at the desired colors, more than 40 mW was, in some cases, obtained from the 2m pre-amplifier.

4.2.1 Different pre-amplifier fiber lengths

As the gain of the two colors is dominant for the short wavelength, this led us to use longer fibers to reduce the ratio difference between the two colors. The spectra in Fig.(4.11) were obtained by amplifying a 4.12 mW input seed by different fiber lengths; 3, 2.9, and 2.8m. The pumping was set at 150 mW for each pump diode, i.e. maximum diode power.

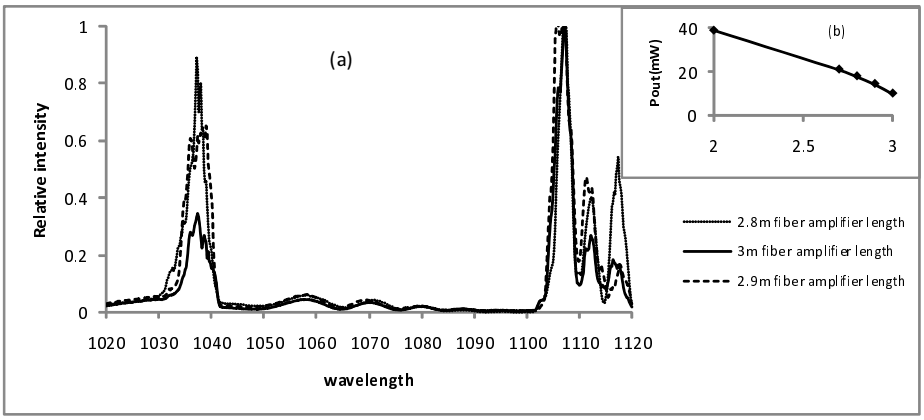

Figure 4.11: a) The amplified spectrum of different fiber lengths; 3, 2.9, 2.8. b) The maximum output average power achieved by the pre-amplifier while changing the fiber lengths.

By pumping firstly a 3m highly doped, single-clad, single mode fiber with the maximum available pumping power (150 mW), the middle region of the fiber might be left without any pumping as most of the pumping power would be absorbed in the few centimeters of the fiber where it inversely populate the large number of atoms (high concentration). As

the amplified short wavelength passes through this region, the fiber re-absorbs the seed and stored as excited atoms. This stored energy would either be partially emited as an incoherent light at longer wavelengths and amplify in the second half of the fiber or be enforced by the incident long wavelength seed to undergo a coherent emission. However, in the case were the incident long wavelength seed intensity is not high to extract most of the stored energy at this wavelength, the ASE will dominate in the output spectrum. This explains the significant presence of ASE in the output spectrum. At this fiber length not much gain was observed at the short wavelength , Fig.(4.11). Only 10 mW was the average output power measured.

For this, shorter fiber lengths (2.9, 2.8, and 2.7m) were examined to achieve the optimal seed amplification for this system. Fig.(4.11) shows that as the fiber gets shorter, the average ouput power increases due to more gain at the short wavelength. The energy difference ratio also decreases. Fig.(4.11-b) represents the maximum average powers that were able to be obtained from the different fiber lengths. Because the ratio of the two colors at 2.8m fiber length is almost equal (2.3/2.5), we chose to cut another 10 cm to help the short wavelength be more amplified. However, the significant presence of the ASE at the ouput of the pre-amplifier (wavelength range 1040 to 1090nm) is due to the low input seed energy of both colors which were not strong enough to extract all the energy stored in the fiber.

4.2.2 Double-ended pumping scheme

The gain of the fiber amplifier depends on three factors: the length of the fiber, the seed and the pump intensity. To have a complete study for this pre-amplifier we had to fix two of these three factors while changing the third one.

The pumping output power characteristics are shown in Fig.(4.12). The graph of the relation between the output ASE power with the pumping from both sides, shows that the ASE power is still increasing with pumping. This means that the state of ASE self saturation has not reached in the fiber. This will lead to a small gain of the signal in amplification.

To illustrate the importance of this double-ended pumping scheme, data were recorded while pumping at different power levels along with a different pumping geometries. The input two-color seed was the one shown in Fig.(4.5). It was of 8.5mW average power. The length of the pre-amplifier used for this study was 2m.

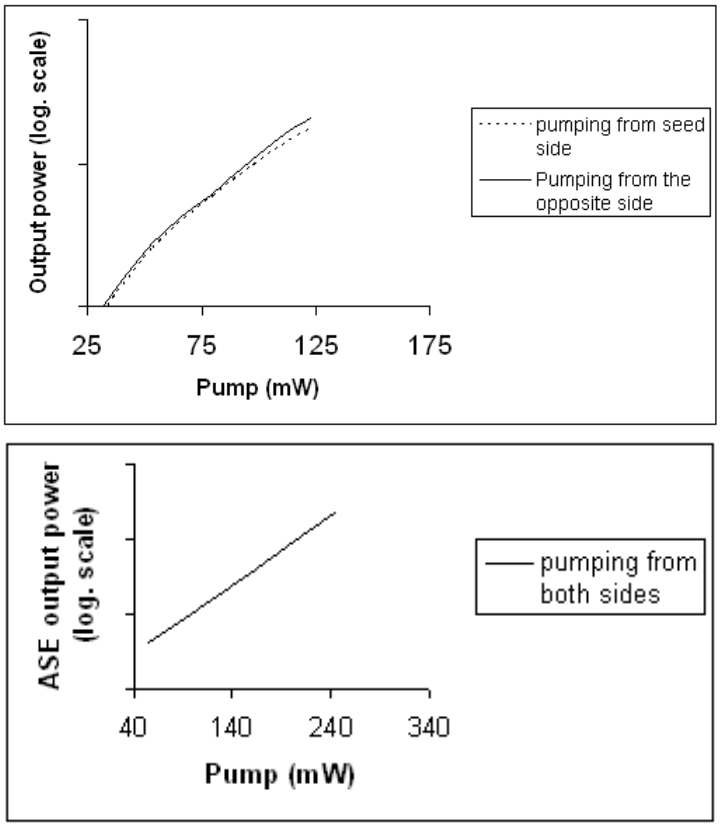

Figure 4.12: The pre-amplifier output. Plot of the ASE power & amplified seed versus the pump input: a) pumping from single side, b) pumping from both sides.

For plots of Figs.(4.13 & 4.14), a single-side of the two pump diodes was set to operate at maximum pumping power while gradually changing the pumping power of the opposite side. This was done as pumping only from one side did not emit enough power for data to be recorded (in the range of micro-watts). In Fig.(4.14), we gradually changed the seed-side pumping values from 0 up to 80 mW, while setting the opposite side of the fiber at maximum pumping level (150 mW). Conversely, Fig.(4.13) was determined. Figs.(4.13 & 4.14) shows the output seed spectra of the two cases. The analysis of these results can be explained as following:

The emission cross-section ratio of the two colors is almost 10 to 1 for short wavelength over the long wavelength. Because of this, most of the average power recorded out from this 2m short pre-amplifier fiber usually came from the short wavelength. However, when

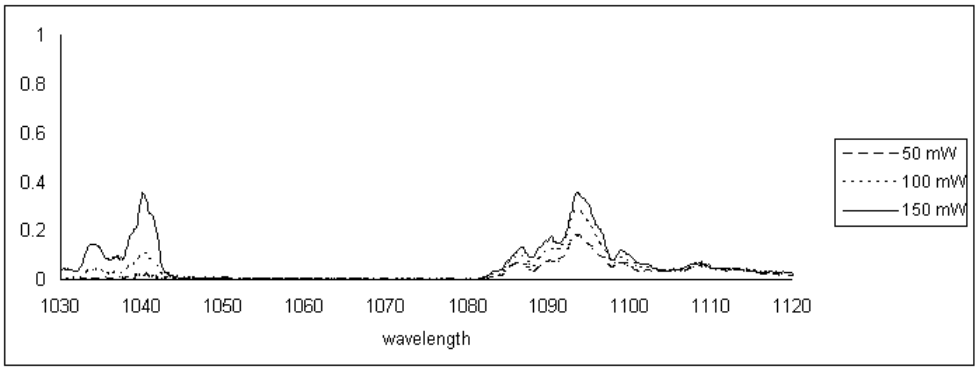

Figure 4.13: Amplified seed spectrum after gradually changing pumping power from the opposite seed input side while having max. pumping (150 mW) from the same side .

the pumping power from the seed side is not high enough to significantly reach half the propagation distance covered by the amplified seed in the pre-amplifier core, the short wavelength will be absorbed and not promote much stimulated emission. This will lower the average output power. Concurrently, after the short wavelength became weaker at the other side of the fiber, the gain competition between the two colors becomes less and the long wavelength of less absorption cross section extracts most of the stored energy.

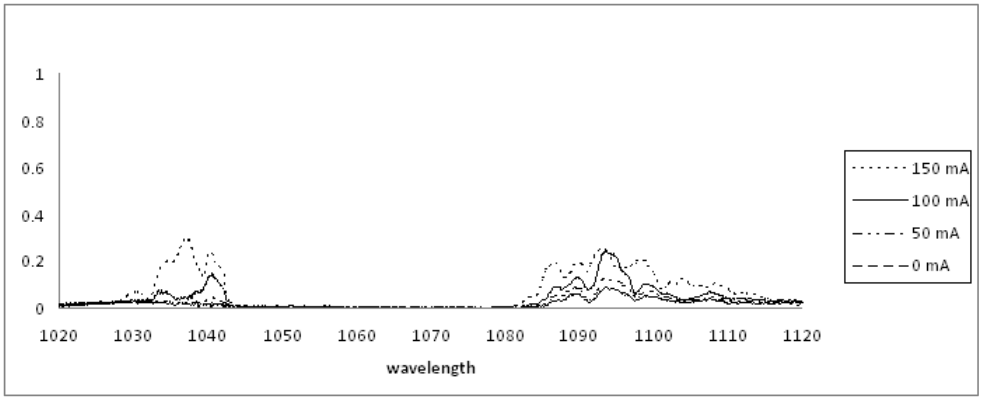

Figure 4.14: Amplified seed spectrum after gradually changing pumping power from the same seed input side while having max. pumping (150 mW) from the opposite side.

The plots show that pumping geometry of Fig.(4.14) gave more energy to long seed bandwidth, this can be referred to the lack of enough pumping power to boost the short wavelength till the other end of the fiber (maximum average power = 7.7 mW). In this

case a significant amount of energy will be extracted at long wavelengths. On the other hand, having the maximum pumping from the seed side, Fig.(4.13), provided more energy for short wavelength to extract energy (maximum average power = 9.24 mW).

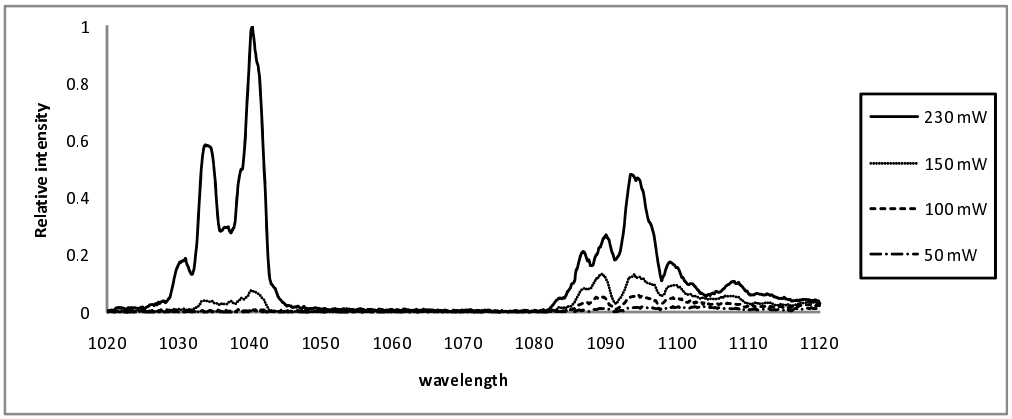

Figure 4.15: Amplified seed spectrum after evenly changing the pumping power from both sides. The notch filter was used for bandwidth isolation .

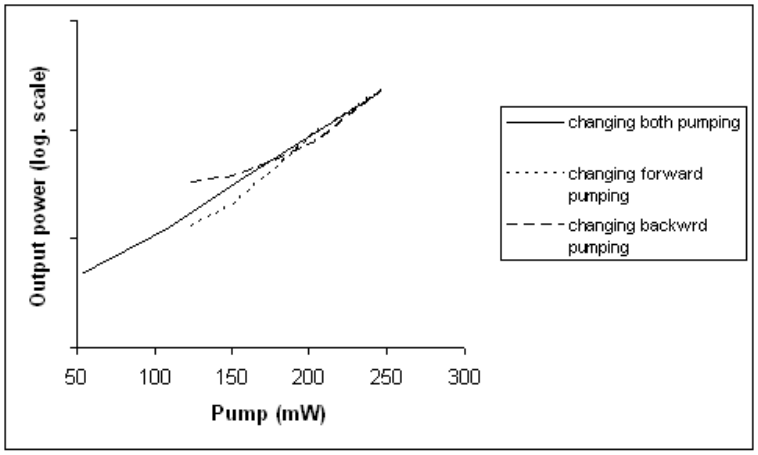

Figure 4.16: Plot of the output seed power versus different pumping power values.

The output average power of the three previous cases is shown in Fig.(4.16). The figure shows that as the pump power increases, the output power increases linearly. The graph shows that the state of saturation has not been reached in the fiber. This means that by simply sending the signal back through for a second pass increases the amplification without

additional pumping. However, with maximum pumping from both sides, a 23 mW output average power was enough power to be sent to the next amplification stages.

The result of these two studies shows that pumping from both ends of the pre-amplifier would give enough power for the short wavelength to boost at the input seed end of the fiber while giving the long wavelength enough gain medium length to be amplified gradually along the fiber.

4.3 Amplifier Configuration

In order to optimze the gain ratio of the two colors, we had to choose the optimal fiber amplifier length for this two color system. The study was done by using three fiber lengths; 5.2, 7, and 9m. The length of the pre-amplifier used for this study was 2m. It should be mentioned that the study made for the amplifier lengths was not possible with the same input two-color seed energy. This is due to the instability of the output spectrum from the PCF. Despite of this, we were able to identify the optimal fiber length of this two-color laser system.

The average backward ASE power was measured while changing the pumping power. For the 5.2m amplifier, the ASE power was 190mW pumping at 6 W, Fig.(4.17).

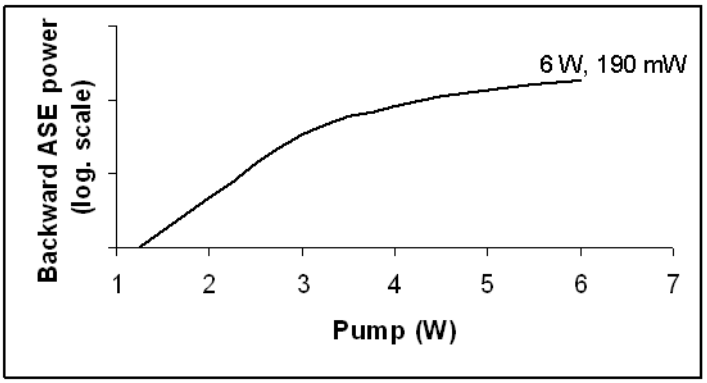

Figure 4.17: Relation of the pumping with the output power.

Fig.(4.18) is the output spectrum of an amplfier chain comprising 2m and 5.2m pre-amplifier and amplifier fiber lengths, respectively.

Pumping at 6.9 W, the average output power after the amplifier was 1.43 W. From Fig.(4.18), it is obvious that most of the stored energy is extracted at the short wavelength.

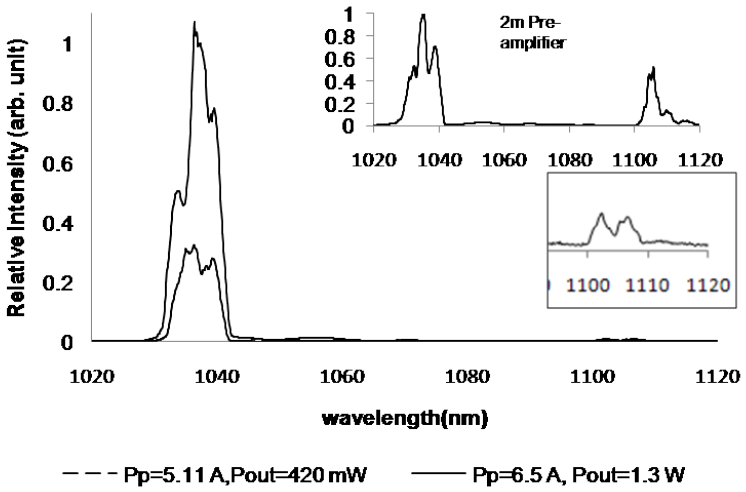

Figure 4.18: The plot of the amplified spectrum after: the 2m pre-amplifier, and the 5m amplifier .

The output power of the long wavelength is in the range of 10 to 20 mW. The power ratio of the two colors is almost 100 to 1. This fiber length is optimal for amplifying the short wavelength. The input amplified signal to this amplifier was strong enough to extract the stored energy at the two colors, and almost no ASE is overlapping with the output spectrum.

Although the average output power is 10 fold the power obtained by waterloo groups [13] & [15], choosing this fiber length is not appropriate to generate mid-infrared radiation as the colors will later pass through different steps and partial loss of amplified power is expected. The signal (long wavelength), will not be high enough to enforce the generation of the idler.

In a trial to improve the gain ratio of the two colors, a 9m fiber amplifier length was used instead. The output average power was 1.07 W.

Fig.(4.19) shows the relation between the pumping power and the backward ASE output power from the 9m amplifier.

The spectrum obtained from this system is shown in Fig.(4.20). By choosing this fiber length, the ratio of the two colors had improved. More stored energy is extracted now at the long wavelength.

To truly measure the average power of the two colors, i.e. blocking any ASE in the

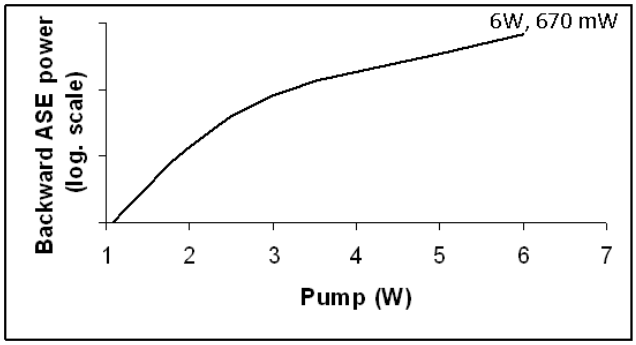

Figure 4.19: Relation of the pumping and the backward ASE output power of the 9m fiber amplifier.

output spectrum, a notch filter was inserted in front of the power meter diode. Pumping with 5.4 W, only 134 mW average power with 10 to 1 energy ratio of the two colors was recorded, while 512 mW with 20 to 1 at 6.9 W.

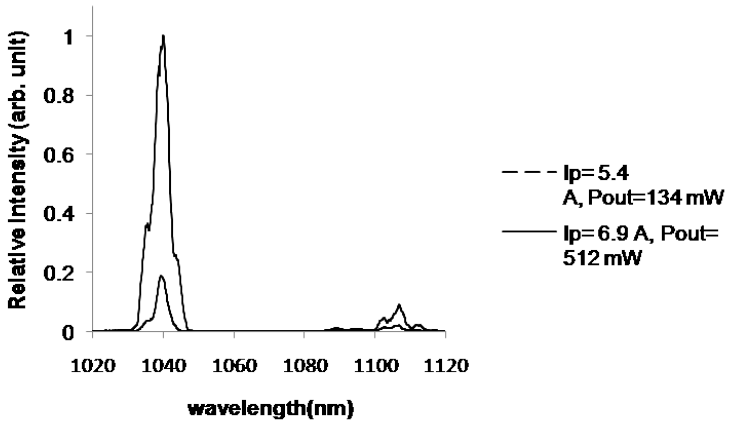

Figure 4.20: The amplified spectrum of a 2m and 9m amplifier chain system.

However, several data were taken for the two previous pre-amplifier and amplifier fiber lengths combination with different input seed energies at the two colors. It showed that the variation of the input energy ratios of the two seed colors has a large impact on the energy ratio of the output spectrum.

The last fiber length chosen was the 7m. The output spectrum is as shown in Fig.(4.21). The gain ratio between the two colors is optimal; it is almost equal. The two colors are

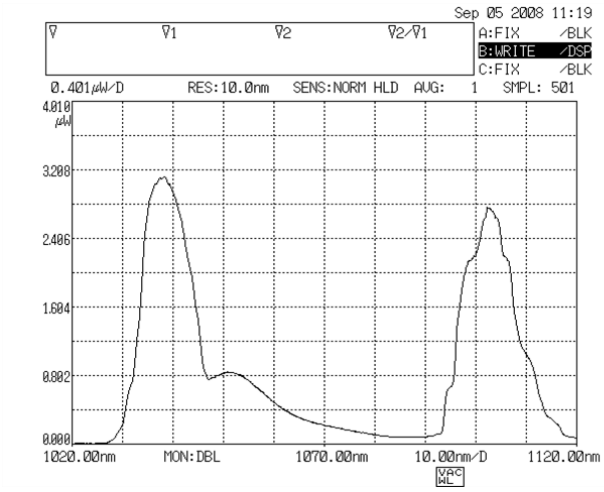

Figure 4.21: The output spectrum after the 7m amplifier.

seventy nanometers apart. The output average power was 740 mW. It can be seen the presence of the ASE in the output spectrum. To measure the output power of the amplified two colors, a notch filter was used to suppress the ASE. The spectrum recorded after the notch filter is shown in Fig.(4.22). 450 mW remained after the notch filter.

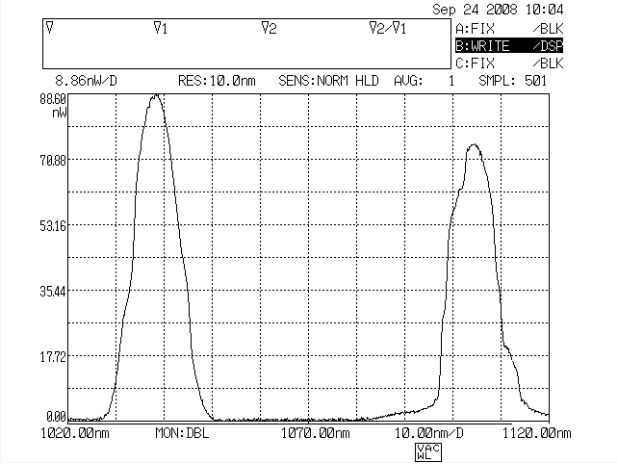

Figure 4.22: The output spectrum after the 7m amplifier.

The big difference in the results with the previous study of the 5.2m and the 9m fiber amplifier lengths was mainly due to the difference in the input seed energy ratio. In order

to equalize the gain ratio, the ratio of the energy of the two colors should be adjusted from the generation of the supercontinuum spectrum.

4.3.1 Two Amplifier-Chain Schemes

The results of using the combination of the 2m pre-amplifier together with the 7m amplifier shows that the output average power has increased seven fold in comparison with the work done by waterloo groups with a better energy ratio between the two colors.

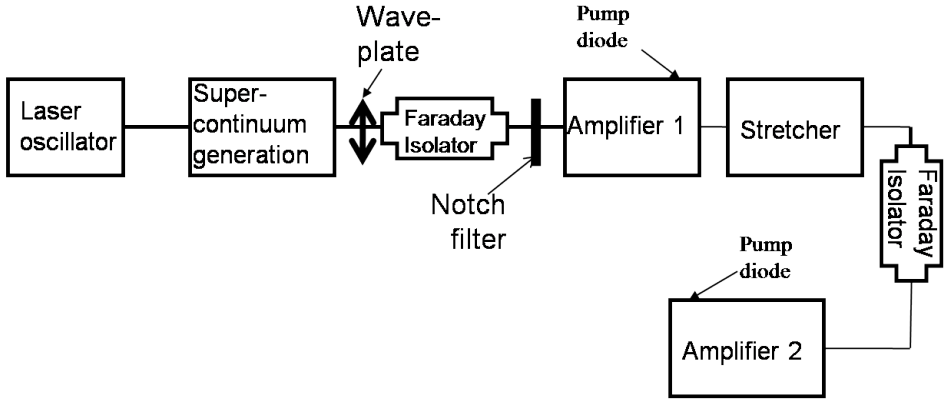

Figure 4.23: Schematic diagram of the two amplifier system.

However, a two-stage amplification scheme by double-clad fibers was also studied in this thesis. This had showed the importance of combining the pre-amplifier together with the amplifier in raising the total average output power of the first stage amplifier.

The schematic diagram of the two amplification stages is shown in Fig.(4.23).

The output power after the PCF was 36mW, and 20mW after the first isolator. To select the two two-color seed of the system, the notch filter was placed after the first isolator. Only 10 mW remained after the selection of the two colors, Fig.(4.24). For the first amplifier, a double-clad fiber was used of 5.2m length.

To improve the gain ratio between the two amplified colors, the spectrum was monitored by the spectrometer while the wave-plate, the knobs of the mirrors before the PCF, and the notch filter were changed to maximize the gain at the long wavelength, the 1105nm. After the first stage of amplification, the average output power was 570 mW. There was a significant amount of ASE in the spectrum. To isolate the ASE from the two colors, a stretcher was imported after the stage amplifier. Only 135 mW remained after the stretcher.

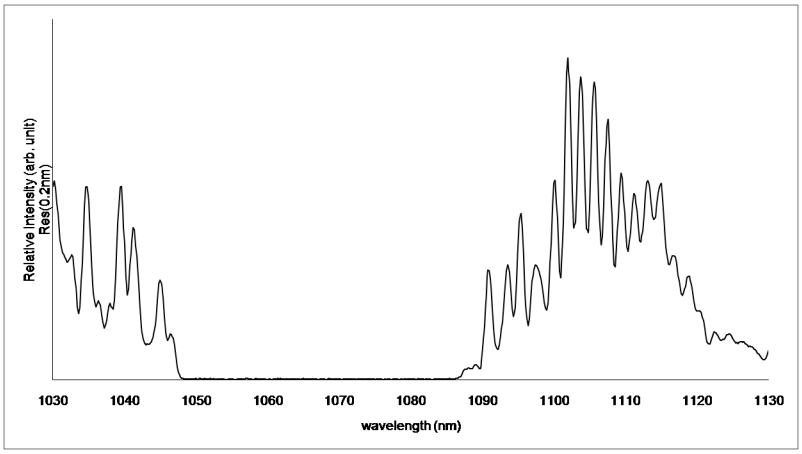

Figure 4.24: The 10 mW two-color seed after the selection by the notch filter.

The spectrum of the two colors is shown in Fig.(4.25).

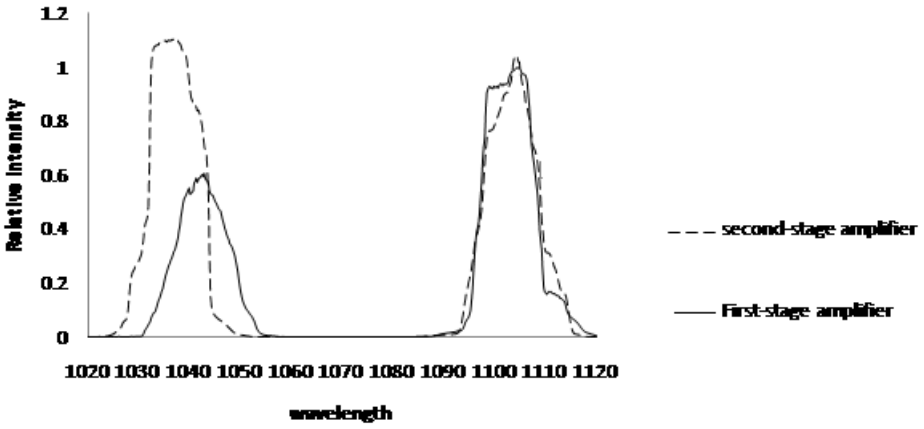

Figure 4.25: The relative intensity of the two colors in each amplification stage.

For the second stage amplification, a 4.4m fiber amplifier length was used. This was to improve the amplification at the short wavelength. The spectrum shown in Fig.(4.25) is the output spectrum of this system with 727 mW average power. There was no coupling of the ASE with the two amplified colors.

By changing the input seed energy of the two colors and prefer the amplification for the short wavelength, a different spectra were obtained with different output average power. Fig.(4.26), shows the spectrum after the second-stage amplifier. The total output power of

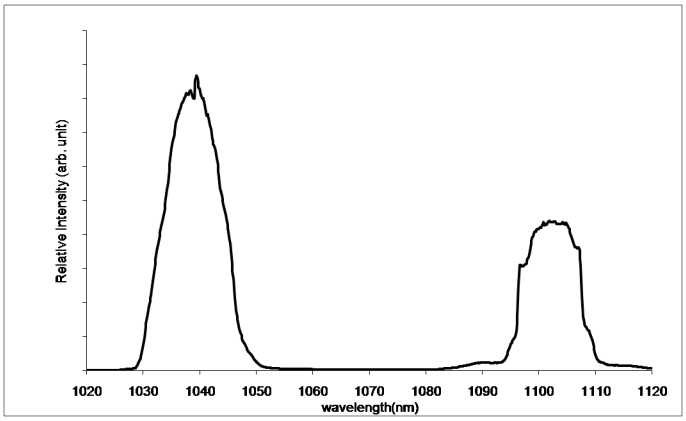

Figure 4.26: The spectrum of the second stage amplifier.

the system was 1.5W.

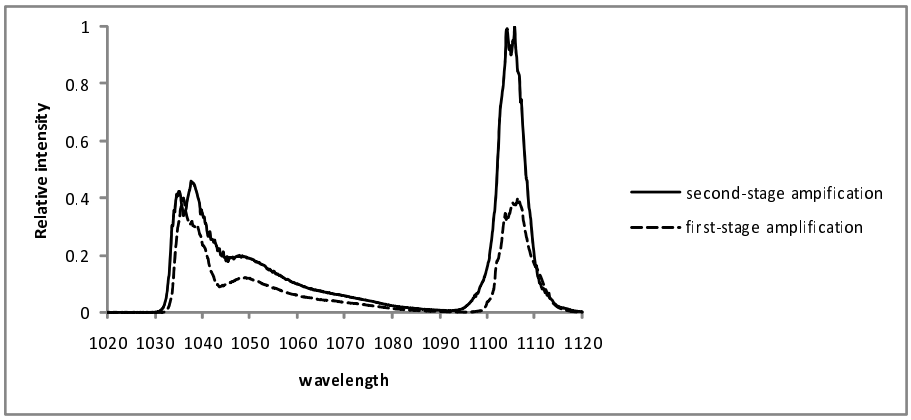

Figure 4.27: Plot of the amplified spectrum by an amplifier chain comprising 5.2 & 9m fiber amplifiers in a two-stage amplification configuration.

In a trial to combine the 5.2m in the first stage of amplification and 9m for the second stage. The output spectrum was obtained as shown in Fig.(4.27). The figure shows that the amplification is operating in a strong ASE regime, where longer fiber lengths actually show worse performance for amplifying the short wavelength due to less competition from ASE. More than 230 mW average power was measured at the output of the second amplification stage.

4.4 Pulse Compression & Autocorrelation

After the accomplishment of building a two color laser system and improving both the gain ratio between the two colors and the total average power of the system, we had finally to recompress the pulses. This part had taken most of the time of the work in this project.

At the beginning we had to demostrate that the compressor-stretcher system and the autocorrelator are functioning properly. For the autocorrelator, the 200fs laser oscillator pulses were sent directly to the autocorrelator. The correlation duration was calculated from the measured line delay:

$$correlation\,duration = \frac{line\,delay = 0.0045cm}{3 \times 10^{10} cm} \times 2 = 300fs$$

To calculate the pulse duration:

$$pulse\,duration = \frac{correlation\,duration = 300}{\sqrt{2}} = 212.12fs$$

To check if the stretcher-compressor system was functioning properly, the 200 fs laser oscillator pulses were stretched by the stretcher to 24ps. This was done by placing all the three gratings of the stretcher at 6 inches away from the lenses of the telescope ($z = z_1 = 6\,inches$). The pulse duration was calculated by using the Treacy equation multiplied by 2 for the double pass in the stretcher:

$$stretched\,duration = \frac{b\,(\lambda/d)\,\delta\lambda}{cd\left[1 - (\lambda/d - sin\theta_i)^2\right]} \times 2$$

$$= \frac{(12 \times 2.54)\,(1.03 \times 1.250)\,10^{-8} \times 1250 \times 10^3}{3 \times 10^{10}\left[1 - (1.03 \times 1.250 - sin41.7))^2\right]} \times 2 = 53.36ps \qquad (4.1)$$

This equation shows that moving gratings by one inch in the stretcher or compressor would stretch or compress pulses by 4 ps, respectively. For the compressor the two gratings were placed at 12 inches separation distance. This distance matches the total separation distance of the gratings in the stretcher. The shortest pulse duration obtained after this system was 235.4fs. The pulse is a bit longer due to the small error that can be easily obtained in our autocorrelator. The line delay measured was 0.005cm for this reading instead of 0.0045cm for the previous case.

To study the effects of the pre-amplifier on the stretching and compression of the pulses,

the stretched short wavelength seed was amplified by the 2 m pre-amplifier. 80 mW was the average output power after the pre-amplifier. The amplified seed was then sent to the compressor. The gratings were placed at half an inch more than the separation distance of the stretcher. They were placed at this distance to compensate the 12 inches of stretching by the stretcher and the normal dispersion formed by the fiber amplifiers. The material dispersion caused by a silica fiber is: -80 ps/nm.km or -0.8 ps/10nm.m [45]. Therefore, using a 2m pre-amplifier fiber would stretch the pulse by 1.6ps. Based on the calculations of Eq.(4.1), almost half an inch is needed to compensate the dispersion formed in this fiber which matches with the experimental work. 533fs was the correlation duration measured after recompressing the short wavelength, Fig.(4.28). However, the correlation duration obtained is almost as twice as the duration obtained for the laser oscillator (300fs). This can be refered to the cubic dispersion generated in the system that limits the system performance. This cubic dispersion arises out of the fiber and the third-order dispersion coefficient of the grating. Both contributions are of the same sign and, therefore, they add up. The wings in the autocorrelation trace have their origin from the seed laser and not an uncompensated higher-order phase contributions of the fiber-stretcher grating-compressor setup.

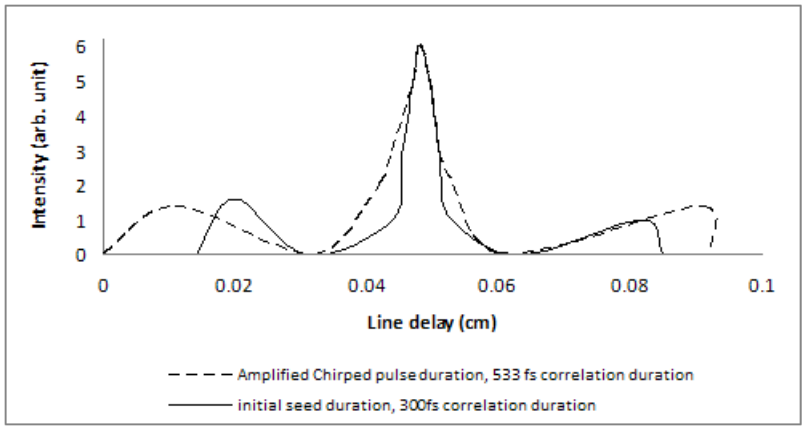

Figure 4.28: Auto-correlation width of both a laser oscillator pulse and the recompressed chirped laser pulses after CPA system.

The stretching and the compression of the long wavelength pulse was not studied at this stage as the power was not high enough to have readings.

After illustrating that both the autocorrelator and the stretcher-compressor are func-

tioning properly, we tried to compress the pulses amplified by the amplifier chain; the 2m pre-amplifier and the 7m amplifier. Starting by the long wavelength, the gratings in the compressor were moved almost 2inches more than the separation distance in the stretcher. This is to compensate the normal dispersion formed by the fiber amplifier lengths. The correlation width measured by the autocorrelator was 533fs. However, the problems of this experiment appeared when we tried to recompress the short wavelength pulses. We were not able to bring the pulses back to the femtosecond duration. The shortest pulse duration that we were able to measure was 13 ps. To further stretch the seed pulses to avoid any possible nonlinear interaction to take place in the amplifiers, the gratings were placed at 2 inches from the telescope lenses; the maximum amount of stretching by the stretcher. This would stretch the pulses by 89ps. Also, a 50 m of undoped fiber was connected to the Yb doped pre-amplifier fiber which also would give a 40ps of stretching, Fig. (4.29). In total, the pulse would be stretched by 129 ps, therefore gratings of compressor should be placed around 29 inches away from each other.

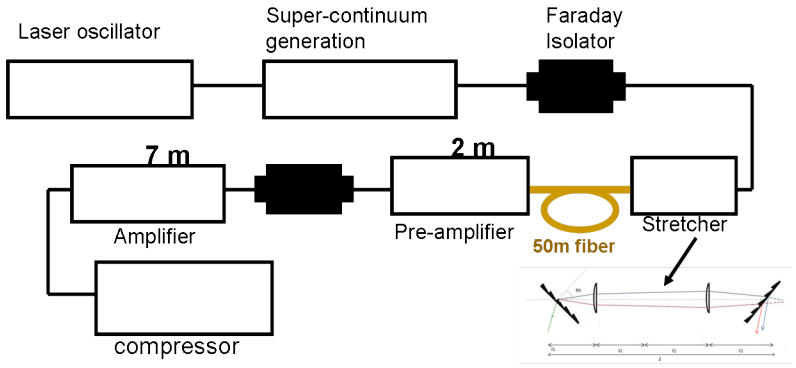

Figure 4.29: The schematic diagram of the maximum amount of stretching done in this experiment.

However, despite all this stretching, the compression achieved was still far away from the 533 fs correlation duration obtained for the long wavelength. Fig.(4.30), gives examples of the correlation duration of the compressed short wavelength pulses obtained at different grating separation distances. However, these results are some of many data were taken. Most of the recorded data were not showing the acceptable autocorrelation pulse shape. The autocorrelation trace had many fluctuations.

For the pulses amplified by the combination of 2m pre-amplifier and 5.2m amplifier, the shortest correlation duration obtained for the recompressed short wavelength pulses

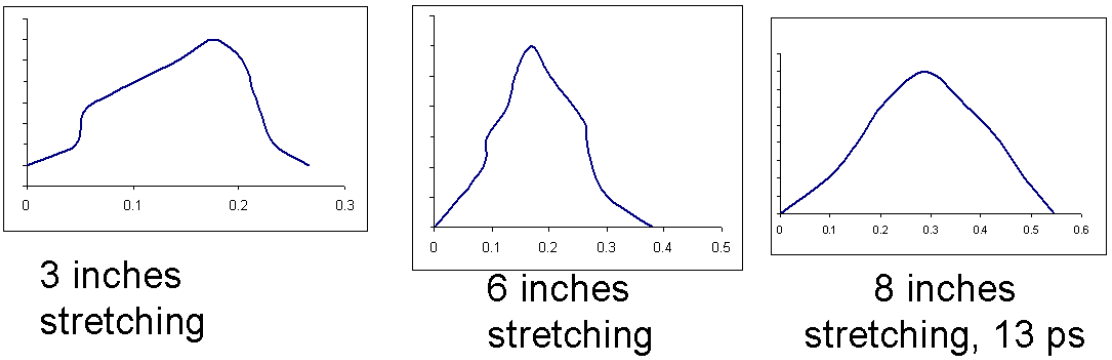

Figure 4.30: Examples of different correlation pulse duration obtained after compression.

was 666fs correlated duration. This pulse duration is almost three times longer than the duration obtained for the laser oscillator pulses. For the pulses amplified by 9m fiber amplifier, the 9ps duration was the shortest duration that we were able to recompress the pulses to. The correlation width obtained is shown in Fig.(4.31). It has to be mentioned that this figure is one from many trials in having a reading that make sense. Most of the readings taken was as if their is an enormous amount of noise and the autocorrelation was as if it was almost flat.

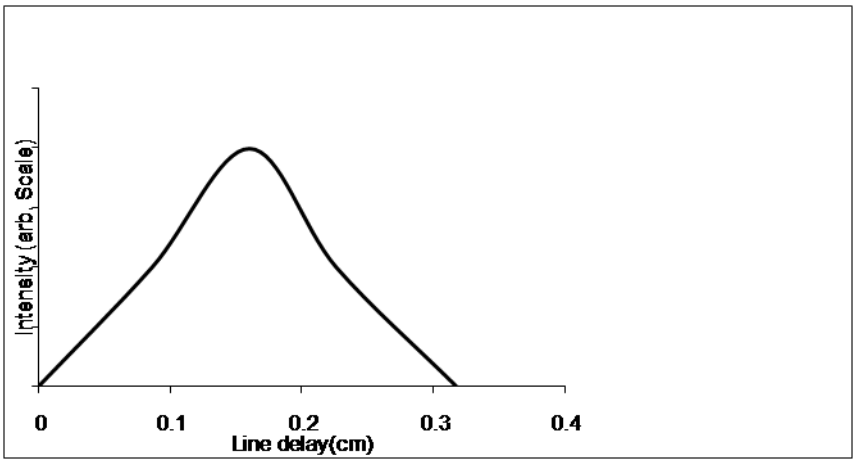

Figure 4.31: The correlation width of the short wavelength pulses amplified by the combination of 2m pre-amplifier and the 9m amplifier.

The compression of the pulses amplified by the two-stage amplifiers, Figs.(4.25&4.27), were also studied. As before, there was no problem in recompressing the long wavelength

pulses. The shortest duration measured was 533 fs correlation duration. For the short wavelength pulses, in the case of combination of 5.2m and 4.4m fiber lengths, we were not able to recompress the pulses to shorter than 8.2 ps correlation duration. For the combination of the 5.2m and 9m fiber lengths, the correlation duration for the long wavelength was 533fs while for the short wavelength, the durations measured had many fluctuations and the line delay was longer than it could be read using the translation axis, where the right angle mirror of the autocorrelator was mounted on to measure the line delay.

With the problem of the recompression of the short wavelength pulses we had to search for the source of this drawback. To accomplish this, only the short wavelength was stretched, amplified and recompressed by the CPA system. The schematic diagram of the experiment is as shown in Fig.(4.32). The fiber lengths used in this experiment were optimal for amplifying the short wavelength.

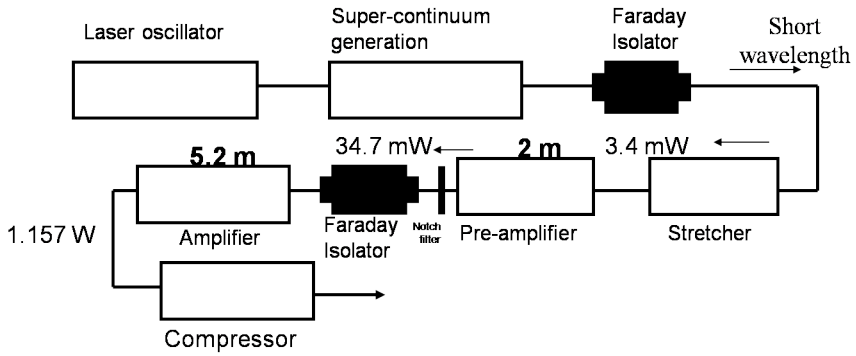

Figure 4.32: The schematic diagram of the amplification of the short wavelength.

After stretching the short wavelength pulses, only 3.4 mW left of the short wavelength from the 15 mW originally incident into the stretcher. The short wavelength was coupled to the 2m preamplifier fiber. The output average power was 34.7 mW. A notch filter was placed after the pre-amplifier to isolate any ASE coupled with the output spectrum. For the amplifier, 5.2 m fiber length was used to amplify the pulses to 1.157 W average power. This output power was measured at maximum pumping power (6.9 W). In this experiment the correlation duration was measured while changing the pumping power. This was done to check if the self-phase modulation is taking placing during the amplifcation.

Fig.(4.33), shows the output results of the durations of the pulses as a function of the pumping power. The figure shows that the pulse duration is almost fixed at 660fs as the pumping power is raised. The slight difference in the readings is due to the error of the

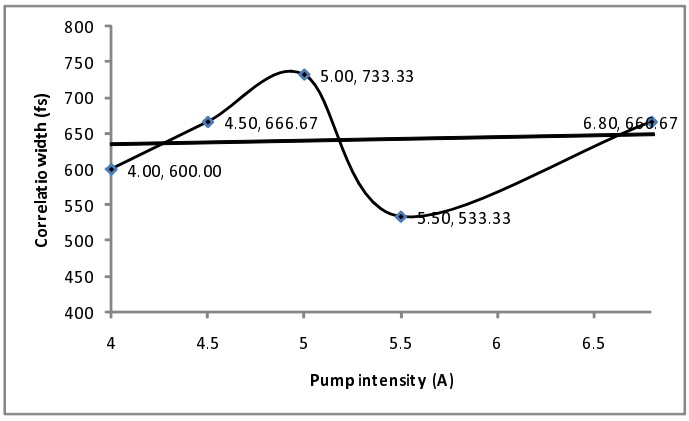

Figure 4.33: The plot of the pump intensity with the correlation width measured at fixed separation grating distance of the compressor.

alignment each time we tried to move the gratings forward and backward to check if the separation distance is still optimal for the compression of the pulses with changing the pumping power. These readings were recorded when the notch filter was placed before the amplifier to isollate the ASE generated by the pre-amplifier. However, when the notch filter was removed, the shortest pulse duration obtained was 1.33ps.

4.5 Doubling frequency of the compressed pulses

From all the above results, we concluded that the reason that the short wavelength pulses are not recompressed back to initial pulse duration might be that there is an overlapping between the short wavelength and the ASE formed in the amplification stages. To demonstrate this understanding we had to do the doubling frequency which is proportional the square of the intensity of the signal.

We first doubled the frequency of the 53 mW seed laser oscillator. By measuring the SHG of the initial seed oscillator pulses, only 1.9 μW was detected of the green color. This reading was used as a reference to compare the results obtained in the experiment for the power of the SHG of the amplified colors. As the intensity of the SHG is proportional to the square of the intensity of the signal, raising the input power 10 times should result in increasing the green color 100 times. The doubling efficiency should be up to 10 % of the input average power. For the recompressed pre-amplified seed laser at the short wavelength of 31.5 mW average output power after the CPA system, 1.18 μW was detected

(recompressed pulse duration is 467fs).

To check if the energy shown in Fig.(4.18) is a gain at the short wavelength, a second-harmonic generation (SHG) was measured at two different average output power levels. 114 μW of green color was measured from a 420 mW while 1.3 mW of green color was detected from 1.43W. The 1.43 W is 30 fold the power used to measure the SHG of the laser oscillator pulses (53mW). This means the green color power, the 1.9 μW , must increase 900 times. In other word, the green color must be 1.7 mW, according to our results, from the 1.43 W. Although these results are not optimal, they are considered close enough to the expected output green color from this system.

For the experiment done in Fig.(4.20), despite the average output power was recorded as 1.07 W only a few micro-watts, instead of milli-watts expected according to the reading of the SHG of the oscillator pulses, of green color from the short wavelength was detected after the SHG crystal. This can be explained as most of the gain at short wavelength appears in Fig.(4.20) is a gain of the ASE coming from the pre-amplifier and no real gain for the short wavelength input seed.

For the experiment in Fig.(4.29) above 1.074 mW of short wavelength SHG green color was detected from a 1.157 W input power.

To summarize the measurments of the SHG, the readings are listed as following:

- 53 mW of seed oscillator: 1.9 µW
- 31.5 mW of seed from 2m pre-amplifier CPA: 1.18 µW
- 1.157 W of 2m pre-amplifier & 5.2m amplifier: 1.074 mW
- 740 mW of 2m pre-amplifier & 7m amplifier: 40 µW
- 1.07 W of 2m pre-amplifier & 9m amplifier: 23 µW

This proved that when blocking ASE and choosing fiber lengths appropriate to amplify the 1035nm, the frequency doubling efficiency is within the expected range. The results can be explained as that when not prefering the gain for the short wavelength by choosing the optimal fiber length for this wavelength, an overlapping of ASE with the short wavelength occurs. For this, the bandwidth of the short wavelength becomes tiny, which by turn lower the efficiency of the SHG and the ability of recompression.

Chapter 5

Summary and Conclusion

A dual-wavelength Chirped pulse amplification fiber amplifier was constructed at 1035nm and 1105nm. A two stage configuration, one with single-clad and the other with double-clad fiber amplifiers, was implemented in hope of producing more power at the two colors. A chirped pulse amplification technique was used to select the two colors and recompress the amplified pulses at the output of the system. To counteract the gain competition of ASE with the amplified seed, a much higher input seed energy of the two colors were generated by supercontinuum generation in a photonic crystal fiber. In addition, the double-ended pumping scheme in a pre-amplifier provided much higher seed energy to be incident into the amplifier stage. With more radiation at the desired colors, the 1035nm and 1105nm, and with shorter pulse duration, the efficiency of the mid-infrared radiation at 18 μm was expected to improve.

Despite these efforts and expectations, the efficiency of the system was not as high as expected. Because these shortcoming, only few microwatts of 500nm radiation was observed by the frequency doubling of the short wavelength (1035nm) when trying to improve the ratio difference of the two color seed energy. This was obtained when using the 7m and 9m fiber amplifier lengths. Although not discussed here, several routes for investigating into the creation of more 500nm radiation were followed such as changing the size of the incident beam and using different focal length lenses. This as well did not significantly improve the efficiency of the outcoming. Although the system exhibited high output power at 1035nm , the 500 mW it produced at this wavelength should have been enough to warrant tens of milliwatts of 517.5nm. The fact that only few micowatts was observed of green radiation leaves the suspect that not much high seed energy was indeed amplified by this system.

Perhaps if simulations of the optimal fiber lengths required for amplifying the two colors was worked on from the beginning, this would partially help in improving the efficiency of this system. However, due to the unstable seed spectrum we had at the time of the study, this had signficantly slowed down the progress of this project and made it difficult to examine experimentaly the optimal fiber lengths for this system. Although the seed source provided more energy of the two colors, the average seed power is still relatively low for this system to extract enough energy and strongly compete the ASE at 1040nm during amplificaiton. When coupling a 6.6 mW of short wavelength seed with the pre-amplifier, we were able to have more than 60 mW output average power. If a supercontinuum laser system can generate a two-color seed, one of 10 nm bandwidth centered at 1035nm and the other of 10 nm bandwidth centered at 1105nm, each of average power 6 mW, then the pre-amplifier system should provide around 60mW input power into the next amplifier stage. If another broad-band spectrum source is available which provide a daily fixed emission of the two colors energy through the whole study period this would give a better chance for comparison between different fiber lengths for optimal amplification.

More complicated issues arise when attempting to shorten the duration of the output pulses. The duration of the amplified short wavelength was not optimally brought back to its initial duration. Using the amplifier stage directly, without any pre-amplification, did not provide a strong seed energy at 1035nm, and thus we were not able to bring back the pulse into its Fourier Transform-limited duration. This is due to the overlapping of 1035nm seed with the ASE developed in the two stages. This explains also why not high output power of green color was obtained from the double frequency of the short wavelength. This conclusion was illustrated when amplifying a single seed color of short wavelength through the whole system (stretcher-compressor, pre-amplifier and amplifier system) while optimizing both the seed energy and fiber lengths. This presents the pre-amplifier as an essential part not only for improving the gain ratio of the two colors, but for the CPA to function properly for this type of system. Also, during this illustration we recognised the importance of the perfect isolation of the two colors in between amplification stages in recompressing the amplified pulses rather than the system efficiency. Because we were using an interference filter for bandwidth isolation, the notch filter also lowered at the same time the energy of the two colors. Perhaps using a better filters would counteract the overlapping phenomena, i.e. the re-compressing problem.

The fiber used in pre-amplifier had high absorption at the pump wavelength and much of the pump power was absorbed with only few microwatts transmited through the other

end of the fiber. Of course more of the seed wavelength was also absorbed, especially if regions in the fiber were not highly pumped. But because only 5 mW of ASE was measured from a single side of this fiber at maximum pump power, 150 mW from both side of the system, this leaves questions of the disappearing of all this energy.

With the rise of fiber lasers, very high power supercontinuum laser systems are being developed of ultrabroad band wavelength using photonic crystal fiber technology. There is some evidence to suggest that using a cw laser oscillator pumping a PCF can produce a supercontinuum generation with 1 mW for each 1nm bandwidth. Perhaps this would give more seed energy at these two colors and improve the efficiency of the whole system. The PCF we used in this project did not have a single-mode patchcord. Because of this we had a significant amount of energy loss in the first passage through the isolator. If another PCF can be connected into a fiber isolator, perhaps this would also help in providing a higher seed energy into amplifier stages. The other suggestion is to amplify the two colors separately in two different fiber lengths and optimize the gain for each color. This system might be more efficient than the one described here, but synchronization loss should be taken seriously in consideration. Also, this would not be compatible with the compactness of the fiber amplifiers. All in all, there are no fiber systems currently available producing a dual-wavelength radiation at these two colors in a single fiber amplifier. For an initial foray into this CPA fiber amplifier system at 1035nm and 1105nm, these results can serve as a useful learning tool to guide our future expectations.

Appendix A

Computer Modeling

The algorithm of this computer program rely on Budz et. al. paper [14]. The Modeling treatment based on the rate equations, provides a good starting point for understanding the two signal amplification in optical fiber. The simulation results should show the changing of the fiber gain for specific wavelengths with the fiber length. These results must illustrate of what have been mentioned in chapter 2.

In order to develop a dual-wavelength fiber laser system, it is essential to develop a model of the experimental setup of the system. The modeling is particularly important in the case of multiple input signals due to the effect of the gain competition in the amplfier. This way, the performance of the dual-wavelength amplifier can be optimized by studying the amplification of the two seed signal in the fiber.

The finite difference method was used to write the algurithm of the program. Several approximations were considered to obtain a simple mathematical mode of propagation of pulses in amplifier. This program was made in a trial to optimize the amplification of the dual wavelength fiber amplifier.

Algorithm A.1 The Algorithm of the choosing the optimal fiber length for input seed wavelengths. This is a transcript of the computer code used to model MRG. It was created in Matlab, and as such any percent signs (%), are commented code, and are ignored in the program. These are used to provide notes.

```
SAp=[2.7 0.19 0.1 0.088 0.08] %%Absorption cross section of pump beam
%% of wavelengths 975, 985, 995, 1005, 1015
SEp=[2.7 0.31 0.25 0.37 0.5]%%Emission cross section of pump beam
%% of wavelengths 975, 985, 995, 1005, 1015
SAs=[] %%Absorption cross sections of seed beam of wavelength 1040
SEs=[] %%Emission cross section of seed of wavelength 1040
SAase=[] %%Absorption cross section of ASE of wavelengths
%% 1000 1010 1020 1030 1040 1050 1060 1070 1080 1090 1100
SEase=[] %%Emission cross section of ASE of wavelengths
%% 1000 1010 1020 1030 1040 1050 1060 1070 1080 1090 1100
LAMDAp=[972.6 973.3 974.5 975.5 976.3]%% Wavelengths of the pump
%% beam in the jth channel
LAMDAs=[1040]%% Wavelength of the seed spectrum
LAMDAase=[1000 1010 1020 1030 1040 1050 1060 1070 1080 1090 1100]%%Wavelength
%% of the ASE in the kth channel
Pp(0)=0.234 %% The pump power at the forward pumping side of wavelength 972.6
PLs(0)=1*e-07 %%Input seed power at z=L
Pzase(0)=0 %%The ase power at z=0
PLase(0)=0 %%The ase power at z=L
h=0.001
L=10
f=L/h %%How many step-size there is in L
j=5 %% Number of channels of pump beam in the L fiber length
v=f/j %% How many step-size for each j pump channel
l=11 %% Number of channels of the ase beam in the L fiber length
e=f/l %% Number of channels for each of the ase channels in the
%% L fiber length
Nt=8*e25
N1(0)=Nt
z=0.001
lamda=1000
alpha=9*e-03
D=2.304*e-03
Cs=0.87
t=8*e-04
k=1
for i=1,f
N2(i-1)=Nt-N1(i-1)
DERp(i-1)= D*(SEp(j)*N2(i-1)-SAp(j)*N1(i-1))*Pp(i-1)-alpha*Pp(i-1)
DERLs(i-1)=-*Cs*(SEs(k)*N2(i-1)-SAs(k)*N1(i-1))*PsL(i-1)+alpha*PsL(i-1)
x=2*h*c*c*10
y=LAMDAase(l)*LAMDAase(l)*LAMDAase(l)
w=x/y
DERzase(i-1)=Cs*(SEase(l)*N2(i-1)-SAase(l)*N1(i-1))*Pzase(i-1)-alpha
*Pzase(i-1)+Cs*SEase(l)*N2(i-1)*w
```

```
DERLase(i-1)=-*Cs*(SEase(l)*N2(i-1)-SAase(l)*N1(i-1))
*PLase(i-1)+alpha*PLase(i-1)-Cs*SEase(l)*N2(i-1)*w
Pp(i)=Pp(i-1)+DERp(i-1)*z
PLs(i)=PLs(i-1)+DERLs(i-1)*z
Pzase(i)=Pzase(i-1)+DERzase(i-1)*z
PLase(i)=PLase(i-1)+DERLase(i-1)*z
z=z+1
M(i)=-*SEp(j)*e-25*Pp(i)*LAMDAp(j)*e-09
O(i)=-*SEs(k)*e-25*PLs(i)*LAMDAs(k)*e-09
Q(i)=-*SEase(l)*e-25*LAMDAase(l)*e-09
B(i)=LAMDAp(j)*e-09*e-25*(SAp(j)+SEp(j))*Pp(i)
G(i)=LAMDAs(k)*e-09*e-25*(SAs(k)+SEs(k))*PLs(i)
T(i)=LAMDAase(l)*e-09*e-25*(SAase(l)+SEase(l))
r=Nt*(D*M(i)+Cs*O(i)+Cs*Q(i)*(Pzase(i)+PLase(i))-(1/t))
u=D*B(i)+Cs*G(i)+Cs*T(i)*(Pzase(i)+PLase(i))+(1/t)
N1(i)=r/u
if (i>v)
    j=j+1;
elseif(j>6)
end
end
    if (i>e)
        l=l+1
    end
```

Bibliography

[1] R. Scheps and J. Myers (1992), Doubly resonant Ti:sapphire laser, IEEE Photonics Technology Letters, vol.4, no.1, pp.1-3

[2] M. R. X. de Barros and P. C. Becker (1993), Two-color synchronously mode-locked femtosecond Ti:sapphire laser, Opt. Lett. 18, 631-633

[3] D. R. Dykaar and S. B. Darack (1993), Sticky pulses: two-color cross-mode-locked femtosecond operation of a single Ti:sapphire laser, Opt. Lett. 18, 634-636

[4] J. M. Evans, D. E. Spence, D. Burns, and W. Sibbett (1993), Dual-wavelength self-mode-locked Ti:sapphire laser, Opt. Lett. 18, 1074-1076

[5] A. Leitenstorfer, C. Fürst, and A. Laubereau (1995), Widely tunable two-color mode-locked Ti:sapphire laser with pulse jitter of less than 2 fs, Opt. Lett. 20, 916-918

[6] R. Scheps and J. F. Myers (1994), Dual-wavelength coupled-cavity Ti:sapphire laser with active mirror for enhanced red operation and efficient intracavity sum frequency generation at 459 nm, IEEE J. Quantum Electron. 30 1050–1057

[7] C. Zhu, Y. Wang, J. He, S. Wang, and X. Hou (2005), Generation and evaluation of synchronous femtosecond and picosecond pulses in a dual-wavelength Ti:sapphire laser, J. Opt. Soc. Am. B 22, 1221-1227

[8] Takashi Onose and Masayuki Katsuragawa (2007), Dual-wavelength injection-locked pulsed laser with highly predictable performance, Optical Society of America

[9] L. Zou et. al. (2006), All-solid-state high power dual-wavelength Ti: sapphire laser, Journal of optoelectronics and Advanced materials Vol. 8, No. 2, p. 843 - 846

[10] Z. Zhang et. al. (2000), Dual wavelength chirped pulse amplification system, Opt. Lett. 25, 581

[11] K.Yamakawa and C.P.Barty (2003), Two-color chirped pulses amplification in an ultrabroadband Ti:Sapphire ring regenerative amplifier , Opt.Lett., 28, 2402

[12] J. F. Xia, J. Song, and D. Strickland (2002), Development of a dual-wavelength Ti:sapphire multi-pass amplifier and its application to intense mid-infrared generation, Opt. Commun. 206,149- 157

[13] Dongfeng Liu, Jie Song, and Donna Strickland (2004), Dual-wavelength ultrashort Yb: fiber amplifier Proc. SPIE, Vol. 5579, 744

[14] A. J. Budz et. al. (2009), Short-Pulse Dual-Wavelength System Based on Mode-Locked Diode Lasers With a Single Polarization-Maintaining Yb:Fiber Amplifier, Journal of lightwave technology, Vol. 27, NO. 16

[15] R. Romero-Alvarez, R. Pettus, Z. Wu, and D. Strickland (2008), Two-color fiber amplifier for short-pulse, midinfrared generation," Opt. Lett., vol. 33, pp. 1065–1067

[16] L. Goldberg et. al. (1998), Mid-infrared difference-frequency generation source pumped by a 1.1–1.5-m dual-wavelength fiber amplifier for trace-gas detection, Opt. Lett., vol. 23, pp. 1517–1519

[17] U. Strossner et. al. (1999), Single-frequency continuous-wave radiation from 0.77 to 1.73 mm generated by a green-pumped optical parametric oscillator with periodically poled LiTaO3, Optical Society of America

[18] D. Strickland, G. Mourou (1985), Compression of amplified chirped optical pulses, Opt. Commun. 56, 219

[19] O. E. Martinez (1987), 3000 Times Grating Compressor with Positive Group Velocity Dispersion: Application to Fiber Compensation in 1.3-1.6 um region, IEEE Journal of Quantum Electronics, VOL. QE-23, NO. 1

[20] E. B. Treacy (1969), Optical Pulse Compression With Diffraction Gratings, IEEE Journal of Quantum Electronics, Vol. QE-5, NO.9

[21] M. D. Perry and G. Mourou (1994), Terawatt to Petawatt Subpicosecond Lasers, Science, Vol. 264, p. 917

[22] M. D. Perry et al. (1999), Petawatt Laser Pulses, Optics Letters, Vol. 24 , p. 160

[23] A. Galvanauskas and M. E. Fermann (2000), 13-W average ultrafast fiber laser, CLEO, San Francisco, CA, postdeadline paper CDP3

[24] Galvanauskas A., Sartania Z., Bischoff M. (2001), Millijoule femtosecond all-fiber system, Conference on Lasers and Electro-Optics Europe- Technical Digest pp.1-2

[25] J. Limpert et al. (2003), High average power femtosecond fiber CPA system, Opt. Lett. 28 (20), 1984

[26] J. Limpert et al. (2006), High-power ultrafast fiber laser systems, IEEE J. Sel. Top. Quantum Electron. 12 (2), 233

[27] K. Kim et al. (2006), eXtreme chirped pulse amplification – beyond the fundamental energy storage limit of semiconductor optical amplifiers, IEEE J. Sel. Top. Quantum Electron. 12 (2), 245

[28] R. R. Alfano, S. L. Shapiro (1970a) Emission in the region 4000 to 7000 Å via four-photon coupling in glass, Phys. Rev. Lett. 24, 584

[29] Ranka et. al. (2000), Visible continuum generation in air-silica microstructure optical fibers with anomalous dispersion at 800 nm, Opt. Lett. 25, 25–27

[30] J. limpert et. al. (2006) High-Power Ultrafast Fiber Laser Systems, IEEE, Quantum Electronics, Vol 12, 2

[31] Dudely et. al. (2006) Supercontinuum generation in photonic crystal fiber, Review Lett. of Modern Physics, Vol. 78

[32] Alfano, Robert R., The Supercontinuum Laser Source: Fundamentals with Updated References (New York, NY : Springer, 2006)

[33] G. P. Agrawal, Nonlinear Fiber Optics (Academic, San Diego, Calif., 2001) Ch2, 4, 6

[34] Robert W. Boyd, Nonlinear Optics,Second Edition (Elsevier science (USA), 2003)

[35] Franz X. Kaertner (2005), Ultrafast Optics, Lecture notes at Massachusetts Institute of Technology (MIT) OpenCourseWare

[36] M. Fermann, A. Galvanauskas, G. Sucha (2001), ULTRAFAST LASERS Technology and Applications, Marcel Dekker, New York

[37] Chuang, Y.-H. Zheng, L. Meyerhofer, D.D (1993), Propagation of light pulses in a chirped-pulse-amplification laser, Quantum Electronics, IEEE Journal of Volume 29, Issue 1, Page(s):270 - 280

[38] S. Kane and J. Squier (1997), Grism-pair stretcher–compressor system for simultaneous second- and third-order dispersion compensation in chirped-pulse amplification, J. Opt. Soc. Am. B 14, 661-665

[39] R. Pachotta, J. Nilsson, A.C. Tropper, and D.C. Hanna (1997), Ytterbium-doped fiber Amplifiers, IEEE J. Quantum Electron, vol. 33, pp. 1049-1056

[40] Mark Csele, Fundamentals of light sources and lasers, (John Wiley & Sons, Inc, 2004)

[41] A. Hardy and R. Oran (1997), Signal Amplification in Strongly Pumped Fiber Amplifiers, IEEE J. of Quantum Elec. 33, page 307

[42] Giuoco, Frank Joseph (December 2003). Construction of a 1014.8nm fiber amplifier for quadrupling into the UV. Master's thesis, Texas A&M University. Available electronically from http : / /handle .tamu .edu /1969 .1 /77 .

[43] G. Agrawal (2007), Nonlinear Fiber Optics, Fourth Edition (Optics and Photonics), Elsevier, Inc. All rights reserved.

[44] Appliction notes, Crystal fiber company, http://www.nktphotonics.com

[45] Gerd Keiser, Optical Fiber Communication, thrid edition, (October 1999)